The Chang–Refsdal Lens Revisited

Jin H. An[1,2⋆] and N. Wyn Evans[2⋆]
[1]*MIT Kavli Institute for Astrophysics & Space Research, Massachusetts Institute of Technology, 77 Massachusetts Avenue, Cambridge, MA 02139, USA*
[2]*Institute of Astronomy, University of Cambridge, Madingley Road, Cambridge, CB3 0HA, UK*

to appear in *Monthly Notices of Royal Astronomical Society*

ABSTRACT
This paper provides a complete theoretical treatment of the point-mass lens perturbed by constant external shear, often called the Chang–Refsdal lens. We show that simple invariants exist for the products of the (complex) positions of the four images, as well as moment sums of their signed magnifications. The image topographies and equations of the caustics and critical curves are also studied. We derive the fully analytic expressions for pre-caustics, which are the loci of non-critical points that map to the caustics under the lens mapping. They constitute boundaries of the region in the image domain that maps onto the interior of the caustics. The areas under the critical curves, caustics and pre-caustics are all evaluated, which enables us to calculate the mean magnification of the source within the caustics. Additionally, the exact analytic expression for the magnification distribution for the source in the triangular caustics is derived, as well as a useful approximate expression. Finally, we find that the Chang–Refsdal lens with additional convergence greater than unity (the 'over-focusing case') can exhibit third-order critical behaviour, if the 'reduced shear' is exactly equal to $\sqrt{3}/2$, and that the number of images for N point masses with non-zero constant shear cannot be greater than $5N - 1$.

1 INTRODUCTION

The so-called Chang–Refsdal lens was put forward to describe the lensing effects of stars in a background galaxy (Chang & Refsdal 1979, 1984). The star acts as a point-mass lens, while the galaxy provides a background perturbation field, which can be approximated by a tidal term to lowest order. The Chang–Refsdal lens is therefore the simplest description of lensing by a tidally perturbed point-mass. As such, it has found widespread astronomical applications – e.g. in the modelling of binary microlensing lightcurves (Gould & Loeb 1992; Gaudi & Gould 1997), in the analysis of the statistics of high-magnification events caused by stars in foreground galaxies (Schneider 1987), and in the study of microlensing of stars around the black hole in the Galactic Centre (Alexander & Loeb 2001), and so on.

The Chang–Refsdal lens is of outstanding physical importance, but it also has a number of elegant mathematical properties, primarily because the 'deflection function' is a rational function of position in the lens plane. Although there has already been much work done on the structure of the caustics and critical curves (Chang & Refsdal 1984; Subramanian, Chitre, & Narasimha 1985; Schneider, Ehlers, & Falco 1992), many of the properties of the Chang–Refsdal lens do not appear to be in the literature. The purpose of this paper is to give a compendium of those results.

The paper is organized as follows. Section 2 presents the Chang–Refsdal lens utilizing the complex notation popularized by Witt (1990; see also Bourassa & Kantowski 1975). In section 3, the lens equation is converted into the imaging polynomial, the roots of which include the image locations. Provided that the source lies within the caustic – so that the number of images is four – then there exist invariants, such as the products of the image positions or the sums of the magnifications weighted by powers of the positions. Section 4 considers two cases when the lens equation is solvable via elementary means, namely when the source lies on one of the axes of the symmetry. In section 5, the pre-caustics of the Chang–Refsdal lens are isolated, together with the critical curves and the caustics. This enables us to calculate in section 6 the mean magnification of the 4-image configurations, and the exact form for a certain conditional distribution of magnifications. Finally, sections 7 and 8 consider two generalizations of the Chang–Refsdal lens, namely the cases of a convergent background and of N point masses with shear. We find that, with the convergence greater than unity, the number of images is either nil or two if the 'reduced shear' is smaller than $\sqrt{3}/2$, nil, two, or four if it is in between $\sqrt{3}/2$ and the unity, and two or four if it is greater than unity. As for N point masses with shear, we establish that the maximum number of possible images are bounded by $5N - 1$.

2 THE LENS EQUATION

The lowest order effect of the tidal field caused by the external mass distribution on gravitational lensing is usually described by a quadratic function that approximates the potential caused by the external masses. Here, we assume that there is no external mass locally, i.e., $\nabla^2\psi_{\rm ext} = 0$ (zero local convergence; see section 7 for the discussion regarding the generalization when $\nabla^2\psi_{\rm ext} = 2\kappa \geqslant 0$).

⋆ E-mail: jinan@space.mit.edu (JA), nwe@ast.cam.ac.uk (NWE)

Then, the lensing potential $\psi_{\rm ext}$ due to the external mass distribution may be approximated to be $\psi_{\rm ext}(x_1, x_2) = \gamma_{\rm R}(x_1^2 - x_2^2)/2 + \gamma_{\rm I} x_1 x_2$, which is actually the most general form of a quadratic function satisfying Laplace's equation. (The constant term in the potential has no physical consequence whilst the linear terms lead to a constant deflection, which can be ignored by introducing the 'offset' between the coordinate origins for the source and the image position.) If a point-mass lens is present under the influence of this tidal field, the whole system is described by the total potential $\psi = (1/2)\ln(x_1^2 + x_2^2) + \psi_{\rm ext}$, which is a superposition of the point-mass potential and the external potential. Here, the coordinate origin in the lens/image plane is defined by the line of sight towards the lens, and the unit of the angular measurement is given by the 'Einstein ring' radius corresponding to the mass of the point-mass lens.

Then, since the deflection angle is the gradient of the lensing potential, we find the lens equation ($\boldsymbol{y} = \boldsymbol{x} - \boldsymbol{\nabla}\psi$):

$$\begin{pmatrix} y_1 \\ y_2 \end{pmatrix} = \left(1 - \frac{1}{x_1^2 + x_2^2}\right)\begin{pmatrix} x_1 \\ x_2 \end{pmatrix} - \begin{pmatrix} \gamma_{\rm R} & \gamma_{\rm I} \\ \gamma_{\rm I} & -\gamma_{\rm R} \end{pmatrix}\begin{pmatrix} x_1 \\ x_2 \end{pmatrix}, \qquad (1)$$

or more compactly, utilizing the complex number notation (Bourassa & Kantowski 1975; Witt 1990)

$$\zeta = z - \frac{1}{\bar{z}} - \gamma\bar{z}. \qquad (2)$$

This is usually referred to as the Chang–Refsdal lens, after Chang & Refsdal (1979, 1984). Here, $\boldsymbol{y} = (y_1, y_2)^{\rm T}$ and $\boldsymbol{x} = (x_1, x_2)^{\rm T}$ are the vectors representing the angular positions of the source (in the absence of the lensing) and of the image, respectively, whereas $\zeta = y_1 + {\rm i}y_2$ and $z = x_1 + {\rm i}x_2$ are their complexified variables. Here, we use the overbar notation to denote the complex conjugation, e.g. $\bar{z} = x_1 - {\rm i}x_2$. In the lens equation, the effect of the tidal field is represented by a symmetric traceless tensor, or equivalently the complex number $\gamma = \gamma_{\rm R} + {\rm i}\gamma_{\rm I}$, usually referred to as an external shear. The components of the (external) shear are related to the (external) potential through $2\gamma_{\rm R} = (\partial^2_{x_1} - \partial^2_{x_2})\psi_{\rm ext}$ and $\gamma_{\rm I} = \partial_{x_1}\partial_{x_2}\psi_{\rm ext}$.

The complex lens equation (2) can also be directly derived from the lensing potential by recognizing that the 'complex scattering function' or the 'deflection function' is twice the 'Wirtinger derivative' (e.g. Schramm & Kayser 1995) of the lensing potential with respect to $\bar{z}$, i.e., the lens equation being $\zeta = z - \alpha$ where $\alpha = 2\partial_{\bar{z}}\psi$. It is easy to show that this reduces to equation (2) with the lensing potential of the Chang–Refsdal lens given by $\psi = (1/2)\ln\bar{z} + (1/4)\gamma\bar{z}^2 + {\rm C.C.}$, where C.C. indicates the complex conjugate of the terms in front. In general, the further (Wirtinger) derivatives of α lead to the convergence $\partial_z\alpha$ and the total shear $\partial_{\bar{z}}\alpha$ of the system. Of a particular interest is that, for a null convergent region ($\partial_z\alpha = 0$), the complex conjugate of the deflection function $\bar{\alpha}$ becomes analytic (An 2005). The introduction of point masses to the system only adds isolated poles, and thus, the (complex conjugate of the) deflection function is described by a complex meromorphic (i.e., analytic everywhere except at isolated poles) function for any lens system without a continuous mass distribution. As for the Chang–Refsdal lens, we find that

$$\zeta = z - \overline{s(z)}; \qquad s(z) = \frac{1}{z} + \bar{\gamma}z, \qquad (3)$$

where $s(z)$ is not only a meromorphic function but actually a rational function of z (of degree 2, provided that $\gamma \neq 0$). This implies that the problem of 'solving' the lens equation essentially reduces to finding zeros of a polynomial (see section 3). In addition, we have $\partial_{\bar{z}}\alpha = \overline{\partial_z\bar{\alpha}} = \overline{\partial_z s} = \overline{s'(z)} = -\bar{z}^{-2} + \gamma$, that is to say, the total shear of the Chang–Refsdal lens is simply the sum of the 'internal shear' (i.e., the $-\bar{z}^{-2}$ term) due to the point mass and the constant external shear γ.

We note that it is always possible to choose the direction of the real axis such that γ is a positive real number. In particular, if $\gamma = |\gamma|{\rm e}^{2{\rm i}\phi_\gamma}$ in a given coordinate system, the rotation of the coordinate axis by an angle ϕ_γ with respect to the origin achieves this. The direction defined by ${\rm e}^{{\rm i}\phi_\gamma}$ is in fact one of the eigendirections of the shear tensor, which we shall refer to as the direction of the shear. The eigenvalue of the shear tensor associated with the direction of the shear is $|\gamma|$, which is sometimes just referred to as the shear by itself. Since the shear tensor is real symmetric and traceless, the second eigendirection (defined by ${\rm i}{\rm e}^{{\rm i}\phi_\gamma}$) is orthogonal to the direction of the shear and the associated eigenvalue is given by '$-|\gamma|$.' In the literature, some authors choose the opposite sign convention for the tidal effect term in equations (1) and (2), which causes an ambiguity in the definition for the direction of the shear between the two eigendirections. Our choice follows the usual weak lensing convention such that the direction of the image stretching distortion is along the direction of the shear, but implies that the direction to the mass that causes the tides is perpendicular to the direction of the tidal shear caused by it.

The Jacobian determinant of equation (1), or equivalently,

$$\mathscr{J} = \frac{\partial\zeta}{\partial z}\frac{\partial\bar{\zeta}}{\partial\bar{z}} - \frac{\partial\zeta}{\partial\bar{z}}\frac{\partial\bar{\zeta}}{\partial z} = 1 - \left|\frac{{\rm d}s}{{\rm d}z}\right|^2 = 1 - \left|\frac{1}{z^2} - \bar{\gamma}\right|^2 \qquad (4)$$

defines the area distortion factor under the linearized lens mapping. Hence, the reciprocal of the Jacobian determinant is (the point-source limit of) the ratio of the apparent solid angle covering the lensed image to that of the original source. Since lensing neither creates nor destroys photons (i.e., the surface brightness is conserved), this also provides us with the ratio of the apparent flux of the image to that of the source, in the limit of a point source. When the individual images corresponding to the given source position are not resolved, the total magnification (i.e., the flux amplification factor) is simply given by the sum of individual magnifications over all images.

The point at which $\mathscr{J} = 0$ is known as the critical point, and the loci of the critical points are referred to as the critical curves (e.g. Schneider, Ehlers, & Falco 1992; Petters, Levine, & Wambsganss 2001). In addition, the source position that allows an image at a critical point is referred to as the caustic point, while the curves that are the mapping of the critical curves under the lens equation are the caustics – that is, a caustic point is the point on the caustics. The magnification of the image at the critical point and consequently the source on the caustics is formally infinite. The caustics are also the boundaries between the source positions with different number of images. (The converse is not necessarily true.)

If there exist additional non-critical image positions that also map onto the caustics under the lens mapping, they are sometimes referred to as pre-caustic points. The pre-caustics[1] are the loci of those non-critical points that map onto the caustics under the lens equation (e.g. Rhie 2002; Finch et al. 2002). The pre-caustics form the boundaries of the image positions that are the (pre-)images of the interior of the caustics, whereas the critical curves are the division lines within them between disjoint domains that the image cannot 'cross over'.

[1] Also called the transition loci by some authors

3 THE IMAGING POLYNOMIAL

To find the image positions corresponding to a given source position ζ, equation (2) needs to be inverted for z. The most straightforward route (c.f., Witt & Mao 1995, for the binary lens equation) involves eliminating $\bar{z}$ from equation (2) by means of its own complex conjugate

$$\bar{z} = f(z) = \bar{\zeta} + s(z) = \bar{\zeta} + \frac{1}{z} + \bar{\gamma} z = \frac{1 + \bar{\zeta} z + \bar{\gamma} z^2}{z}. \tag{5}$$

This results in a rational equation of z

$$g(z) = z - \frac{1}{f(z)} - \gamma f(z) - \zeta = -\frac{\sum_{k=0}^{4} a_k z^k}{z(1 + \zeta z + \bar{\gamma} z^2)} = 0 \tag{6}$$

where

$$\begin{aligned} a_0 &= \gamma\,, \\ a_1 &= 2\bar{\zeta}\gamma + \zeta\,, \\ a_2 &= \bar{\zeta}^2\gamma + 2|\gamma|^2 + |\zeta|^2\,, \\ a_3 &= \bar{\gamma}\zeta + 2\bar{\zeta}|\gamma|^2 - \bar{\zeta}\,, \\ a_4 &= \bar{\gamma}(|\gamma|^2 - 1)\,, \end{aligned} \tag{7}$$

that needs to be solved for the image positions. In general, the polynomials in the numerator and the denominator of $g(z)$ as expressed in equation (6) are relative prime, and so the problem reduces to solving a quartic polynomial equation $g_{\rm n}(z) = \sum_{k=0}^{4} a_k z^k = 0$, which in principle can be solved algebraically. The result further implies that the number of the images allowed by equation (2) for a given source position cannot be greater than four.

We note however that $g(z_0) = 0$ is only the necessary, but not the sufficient, condition for z_0 being one of the image positions. In other words, not all of the zeros of $g(z)$ are the solution of equation (2). For instance, if we replace $\bar{z}$ with an unrelated new variable w in equations (2) and (5), and solve for z by eliminating w, then the solution is still found from $g(z) = 0$ for which $w = f(z)$ is not necessarily the complex conjugate of z.[2] Therefore, to restrict the zeros of $g(z)$ to actual image positions, an additional non-algebraic constraint that $\bar{z}_0 = f(z_0)$ where $g(z_0) = 0$ is also required.

We also note that some properties of the Chang–Refsdal lens can be examined through the analysis of the rational function $g(z)$ and the quartic polynomial equation $g_{\rm n}(z) = 0$. For example,

$$\frac{{\rm d}g}{{\rm d}z} = g'(z) = 1 - \left[\gamma - \frac{1}{f(z)^2}\right]\left(\bar{\gamma} - \frac{1}{z^2}\right) \tag{8}$$

so that, if the solution z_0 of $g(z) = 0$ corresponds to an actual image position [i.e., $f(z_0) = \bar{z}_0$], we find that $g'(z_0) = \mathscr{J}(z_0)$. (Here and throughout the paper, the use of the primed symbols will be reserved for the *total* derivative.) Since the magnification must be real, this also implies that $g'(z_0) \in \mathbb{R}$ is the necessary condition for the zero z_0 of $g(z)$ to correspond to an actual image position. In addition, if z_0 corresponds to a critical point, then $g(z_0) = g'(z_0) = 0$, so that z_0 is a degenerate zero of $g(z)$. In other words, if ζ is a caustic point, then the imaging equation $g(z) = 0$ allows a degenerate solution that corresponds to a critical point. Furthermore, $g(z_0) = g'(z_0) = 0$ if and only if $g_{\rm n}(z_0) = g'_{\rm n}(z_0) = 0$, and therefore, the discriminant of the polynomial $g_{\rm n}(z)$ also provides an algebraic equation $D(\zeta_{\rm c}, \bar{\zeta}_{\rm c}) = 0$ for the caustics points $\zeta_{\rm c}$ to satisfy.

We further note that, if z_0 is the critical point that maps to a cusp point on the caustics, $g(z_0) = g'(z_0) = g''(z_0) = 0$ and $g_{\rm n}(z_0) = g'_{\rm n}(z_0) = g''_{\rm n}(z_0) = 0$, and thus that z_0 is a doubly-degenerate solution (i.e., a triple root) of $g(z) = g_{\rm n}(z) = 0$. In fact, if the deflection function is described by an analytic function, we can establish a connection between multiply-degenerate solutions of a certain analytic function derived from the deflection function and higher-order critical behaviour (or 'catastrophe') of the lens mapping at the corresponding point. However, the present analytic function $g(z)$ can at most have a triple root for any $\zeta \in \mathbb{C}$ so that the cusp catastrophe is the critical behaviour of the highest possible order for the Chang–Refsdal lens, provided that $\gamma \neq 0$ and $|\gamma| \neq 1$.

Next, for any rational function $r(z) = r_{\rm n}(z)/r_{\rm d}(z)$ of z, where $r_{\rm n}(z)$ and $r_{\rm d}(z)$ are polynomials with no common factor, we find that there exist linear combinations of linearly-independent polynomials $p_k(z) = [r_{\rm n}(z)]^k [r_{\rm d}(z)]^{4-k}$ $(k = 0, \ldots, 4)$ that are divisible by $g_{\rm n}(z)$. That is, $\sum_{k=0}^{4} c_k p_k(z) = q(z) g_{\rm n}(z)$ or dividing by $[r_{\rm d}(z)]^4$,

$$\sum_{k=0}^{4} c_k \frac{[r_{\rm n}(z)]^k [r_{\rm d}(z)]^{4-k}}{[r_{\rm d}(z)]^4} = \sum_{k=0}^{4} c_k [r(z)]^k = \frac{q(z) g_{\rm n}(z)}{[r_{\rm d}(z)]^4} \tag{9}$$

where $q(z)$ is a polynomial of z. Thus, for any rational function $r(z)$, its values $v = r(z_0)$ at the image positions z_0 are zeros of a quartic polynomial $c(v) = \sum_{k=0}^{4} c_k v^k$, provided that $r(z)$ does not diverge at the image position [i.e., there is no common factor between $g_{\rm n}(z)$ and $r_{\rm d}(z)$]. In particular, if the rational function is given such that $r(z) = R[z, f(z)]$ where $R[z, w]$ is a rational function of z and w that satisfies that $R[z, w] \in \mathbb{R}$ for $w = \bar{z}$, then only the real zeros of $c(v)$ correspond to its values at image positions. Furthermore, if $R[\bar{w}, \bar{z}] = \overline{R[z, w]}$, we can show that, for any non-real zero $v_{\rm c} = r(z_0^{\rm c})$ of $c(v)$ where $z_0^{\rm c}$ is a zero of $g(z)$ that does not correspond to any actual image, its complex conjugate $\bar{v}_{\rm c}$ is also a zero of $c(v)$. Hence, for this case, $c(v)$ is completely factored into linear or irreducible quadratic polynomials with real coefficients, and therefore (after the common scale factor has been taken out) $c(v) = 0$ reduces to a *real-coefficient* quartic polynomial equation, and only its real solutions are valid, which correspond to the actual image positions.

For example, if $R[z, w] = zw$, then $R[z, \bar{z}] = z\bar{z} = |z|^2 \in \mathbb{R}$ and $R[\bar{w}, \bar{z}] = \bar{w}\bar{z} = \overline{zw} = \overline{R[z, w]}$, and so, with $r(z) = R[z, f(z)] = z f(z) = 1 + \bar{\zeta} z + \bar{\gamma} z^2$, there exists a real quartic polynomial equation $\sum_{k=0}^{4} b_k v^k = 0$ whose real solutions are $|z_0|^2$ where z_0 are the image positions. By equating the remainder of the polynomial division of $\sum_{k=0}^{4} b_k (1 + \bar{\zeta} z + \bar{\gamma} z^2)^k$ by $g_{\rm n}(z)$ to be identically nil, we find the real coefficients (up to a common multiplicative scale factor):

$$\begin{aligned} b_0 &= 1\,, \\ b_1 &= -(4 + |\zeta|^2)\,, \\ b_2 &= 6 + 2(|\zeta|^2 - |\gamma|^2) + \zeta^2\bar{\gamma} + \bar{\zeta}^2\gamma\,, \\ b_3 &= -4(1 - |\gamma|^2) - |\zeta|^2(|\gamma|^2 + 1) - (\zeta^2\bar{\gamma} + \bar{\zeta}^2\gamma)\,, \\ b_4 &= (1 - |\gamma|^2)^2\,. \end{aligned} \tag{10}$$

The result implies that, for the 4-image Chang–Refsdal lens system, there exists a relation among the image positions that

$$\prod_{k=1}^{4} |z_k| = \left|\frac{1}{1 - |\gamma|^2}\right| \tag{11}$$

where z_1, z_2, z_3, and z_4 are the complex locations of four images. In fact, this relation can be derived from the stricter relation found from the coefficients of equation (7)

$$\prod_{k=1}^{4} z_k = \frac{\gamma}{\bar{\gamma}(|\gamma|^2 - 1)}. \tag{12}$$

We note that there also exist similar real coefficient quartic polynomial equations for $2\Re[z_0]$, $2\Im[z_0]$, $\cot(\arg z_0)$, $\mathscr{J}(z_0)$ and

[2] However, if $w_0 = f(z_0) \neq \bar{z}_0$ where z_0 is a zero of $g(z)$, then it can be proven that $\bar{w}_0$ is another zero of $g(z)$ distinct from the initial zero z_0. That is, any zero of $g(z)$ that does not correspond to an actual image position always occurs in a pair.

so on (c.f., Asada 2002; Asada, Kasai, & Kasai 2004). In principle, they can be found by entirely algebraic operations outlined above with the choice of the rational function being $z + f(z)$, $\mathrm{i}[f(z) - z]$, $\mathrm{i}[z + f(z)][z - f(z)]^{-1}$, or equation (8), respectively although the actual algebra involved is rather messy.

3.1 Position and Magnification Moments

The fact that $g(z_0) = 0$ and $g'(z_0) = \mathscr{J}(z_0)$ for image positions z_0 implies that certain contour integrals involving $[g(z)]^{-1}$ reduce to the position-magnification moment sum over the all allowed images (Dalal & Rabin 2001; Hunter & Evans 2001), provided that all zeros of $g(z)$ are the actual image positions. Here, we show that this also implies that the series of the position-magnification moment sums are coefficients for particular Taylor-series expansion of $[g(z)]^{-1}$ (see also Evans & Hunter 2002).

First, since $\lim_{z\to\infty}[g(z)]^{-1} = 0$ assuming $|\gamma| \neq 1$, we note that $[g(z)]^{-1}$ has the convergent Taylor-series expansion at $z = \infty$ such that

$$\frac{1}{g(z)} = \sum_{n=1}^{\infty} \frac{C_n}{z^n}; \qquad C_n = \frac{1}{n!}\,\frac{\mathrm{d}^n}{\mathrm{d}z^n}\frac{1}{(g\circ h)(z)}\bigg|_{z=0} \tag{13}$$

where $h(z) \equiv z^{-1}$. Next, let us consider the contour integral

$$\oint_{\partial S_\infty} \frac{z^n\,\mathrm{d}z}{g(z)} = \oint_{\partial S_\infty} \mathrm{d}z\, z^n \left(\sum_{j=1}^{\infty}\frac{C_j}{z^j}\right) = \sum_{j=1}^{\infty} C_j \left(\oint_{\partial S_\infty} z^{n-j}\mathrm{d}z\right)$$
$$= \begin{cases} 2\pi\mathrm{i}C_{n+1} & \text{for } n = 0, 1, \ldots \\ 0 & \text{for } n = -1, -2, \ldots \end{cases} \tag{14}$$

where the integration path ∂S_∞ is taken to be a circle with a radius of infinity. However, the contour integral can also be evaluated using Cauchy's Residue Theorem. Since $g(0) \neq 0$, non-vanishing residue contributions to the integral are at $z = z_0$ where z_0 is a zero of $g(z)$ [i.e., $g(z_0) = 0$]

$$\operatorname*{Res}_{z=z_0}\left[\frac{z^n}{g(z)}\right] = \lim_{z\to z_0}\frac{(z - z_0)z^n}{g(z)} = \frac{z_0^n}{g'(z_0)} \tag{15}$$

for any integer n [also assumed is that none of the zeros of $g(z)$ is degenerate so that $g'(z_0) \neq 0$ when $g(z_0) = 0$], and at $z = 0$

$$\operatorname*{Res}_{z=0}\left[\frac{1}{z^m g(z)}\right] = \frac{1}{(m-1)!}\,\frac{\mathrm{d}^{m-1}}{\mathrm{d}z^{m-1}}\frac{1}{g(z)}\bigg|_{z=0} \tag{16}$$

for a negative integer $n = -m$ ($m = 1, 2, \ldots$). Then, the residue theorem, together with equation (14) indicates that

$$\sum_k \frac{z_k^n}{g'(z_k)} = \begin{cases} C_{n+1} & \text{for } n = 0, 1, \ldots \\ -\mathrm{Res}_{z=0}\left\{[z^{-n}g(z)]^{-1}\right\} & \text{for } n = -1, -2, \ldots \end{cases}, \tag{17}$$

where $z_k \neq 0$, $g(z_k) = 0$, and $g'(z_k) \neq 0$. Here, if all of the z_k's are the solutions of equation (2) – i.e., an actual image exists at every $z = z_k$ – then from $g'(z_0) = \mathscr{J}(z_0)$, the left-hand side of equation (17) is the same as the (signed-)magnification-weighted moment sum over the all images. Furthermore, the formal expressions given in equations (13) and (16) indicate that the sums in equation (17) are also the coefficients for the Taylor-series expansion of $[g(z)]^{-1}$, that is to say,

$$\frac{1}{g(z)} = \sum_{m=1}^{\infty}\frac{\mathrm{d}^m}{\mathrm{d}w^m}\frac{1}{g(w^{-1})}\bigg|_{w=0}\frac{z^{-m}}{m!} = \sum_{n=0}^{\infty}\frac{1}{z^{n+1}}\left[\sum_k \frac{z_k^n}{g'(z_k)}\right] \tag{18}$$

at $z = \infty$, or

$$\frac{1}{g(z)} = \sum_{n=0}^{\infty}\frac{\mathrm{d}^n}{\mathrm{d}w^n}\frac{1}{g(w)}\bigg|_{w=0}\frac{z^n}{n!} = -\sum_{n=0}^{\infty} z^n\left[\sum_k \frac{1}{z_k^{n+1}g'(z_k)}\right] \tag{19}$$

at $z = 0$. We note that this result is reminiscent of Ramanujan's Master Theorem (Berndt 1985), which relates moment integrals and Taylor coefficients.

From the series expansion of equation (6) at $z = 0$ and $z = \infty$, we can derived the following invariant position-moment sums for the Chang–Refsdal lens:

$$\sum_{k=1}^{4}\frac{1}{\mathscr{J}(z_k)} = \frac{1}{1 - |\gamma|^2}; \tag{20}$$

$$\sum_{k=1}^{4}\frac{1}{z_k\mathscr{J}(z_k)} = 0; \qquad \sum_{k=1}^{4}\frac{1}{z_k^2\mathscr{J}(z_k)} = \frac{1}{\gamma}. \tag{21}$$

In addition, we also find that

$$\sum_{k=1}^{4}\frac{z_k}{\mathscr{J}(z_k)} = \frac{\zeta + \gamma\bar{\zeta}}{(1 - |\gamma|^2)^2}; \qquad \sum_{k=1}^{4}\frac{1}{z_k^3\mathscr{J}(z_k)} = -\frac{\zeta + \gamma\bar{\zeta}}{\gamma^2}, \tag{22}$$

which subsequently implies that

$$\sum_{k=1}^{4}\left[z_k(1 - |\gamma|^2)^2 + \frac{\gamma^2}{z_k^3}\right]\frac{1}{\mathscr{J}(z_k)} = 0. \tag{23}$$

Similar results have also been obtained by Witt & Mao (2000) and Hunter & Evans (2001).

4 SOURCE ON THE SYMMETRY AXIS

Although it is in principle possible to solve equation (6) for the image positions with an algebraic technique such as Ferrari's method (e.g. Abramowitz & Stegun 1972) for an arbitrary source position, the actual algebra is rather complicated, if not entirely uninteresting. In fact, for most cases, applying a simple numerical algorithm to solve the given quartic polynomial is more advantageous. However, if the source lies along either of the symmetry axes of the system, the complete analytic solutions are reasonably simple to derive and can be illuminating. For the simplicity of the algebra, throughout this section, we use the lens equation (2) with the real direction given by the direction of the shear (i.e., the tide-causing mass lies along the pure imaginary axis) so that γ is a positive real number (i.e., $\gamma = \bar{\gamma} = |\gamma|$).

4.1 The Real Axis

First, let us think of the case when the source is along the real axis (i.e., $\bar{\zeta} = \zeta$). From the symmetry of the problem, we expect that there will be images along the real axis, too. Since any solution along the real axis satisfies $z = \bar{z}$ and equation (2), we can derive the quadratic equation for z

$$g_{\mathrm{R}}(z) = (1 - \gamma)z^2 - \zeta z - 1 = 0. \tag{24}$$

It is a straightforward exercise to show that $g_{\mathrm{R}}(z)$ is a factor of $g_{\mathrm{n}}(z)$ if $\zeta = \bar{\zeta}$ and $\gamma = \bar{\gamma}$. In particular, we find that

$$g_{\mathrm{n}}(z) = -g_{\mathrm{R}}(z)\left[\gamma(1 + \gamma)z^2 + (1 + \gamma)\zeta z + \gamma\right] \tag{25}$$

and therefore, the solutions of the quartic equation $g_{\mathrm{n}}(z) = 0$ are

$$z_{\mathrm{on}} = \frac{\zeta \pm \left[\zeta^2 + 4(1 - \gamma)\right]^{1/2}}{2(1 - \gamma)},$$
$$z_{\mathrm{off}} = -\frac{\zeta}{2\gamma} \pm \frac{\mathrm{i}}{2\gamma}\left(\frac{4\gamma^2}{1 + \gamma} - \zeta^2\right)^{1/2}. \tag{26}$$

Table 1. Summary of the image properties for the cases when the source lies on the real axis (parallel to the direction of the shear). Here, $A = 4\gamma^2 - (1+\gamma)\zeta^2$ and $B = \zeta^2 + 4(1-\gamma)$.

Shear	Source Position	Images	Total Magnification $M_{\rm tot}$
$0 \leqslant \gamma < 1$	$\lvert\zeta\rvert < 2\gamma(1+\gamma)^{-1/2}$	4 images [2 on (+, +) & 2 off (−, −)]	$\dfrac{4\gamma - (1+\gamma)\zeta^2}{(1-\gamma^2)A}$
$0 \leqslant \gamma < 1$	$\lvert\zeta\rvert > 2\gamma(1+\gamma)^{-1/2}$	2 images [2 on (+, −)]	$\dfrac{\lvert\zeta\rvert(\zeta^2 - 4\gamma + 2)}{(1-\gamma)(-A)\sqrt{B}}$
$\gamma > 1$	$\lvert\zeta\rvert < 2\sqrt{\gamma - 1}$	2 images [2 off (−, −)]	$\dfrac{2\gamma}{(\gamma+1)A}$
$\gamma > 1$	$2\sqrt{\gamma-1} < \lvert\zeta\rvert < 2\gamma(\gamma+1)^{-1/2}$	4 images [2 on (+, −) & 2 off (−, −)]	$\dfrac{\lvert\zeta\rvert(4\gamma - 2 - \zeta^2)}{(\gamma-1)A\sqrt{B}} + \dfrac{2\gamma}{(\gamma+1)A}$
$\gamma > 1$	$\lvert\zeta\rvert > 2\gamma(\gamma+1)^{-1/2}$	2 images [2 on (−, −)]	$\dfrac{\zeta^2 - 2\gamma}{(\gamma-1)(-A)}$

Here, two on-axis solutions $z_{\rm on}$ are image locations if $B \equiv \zeta^2 + 4(1-\gamma) \geqslant 0$. Since $\zeta \in \mathbb{R}$ and $\gamma \geqslant 0$, this happens (i) if $0 \leqslant \gamma < 1$ or (ii) if $\gamma > 1$ and $\lvert\zeta\rvert \geqslant 2\sqrt{\gamma-1}$. On the other hand, the two off-axis solutions $z_{\rm off}$ become physical image positions if $\lvert\zeta\rvert \leqslant 2\gamma(1+\gamma)^{-1/2}$. The corresponding magnifications of the images can be found from equation (4). We remark that the algebra may be eased by reducing the orders of the power of z through the use of quadratic equations (24) and (25) for image positions and by deriving additional quadratic equations for magnification via a similar route using the resultant polynomials, as in section 3. Furthermore, since equation (4) is invariant under complex conjugation, and the two off-axis solutions are mutual complex conjugates, they must have identical magnifications. We find that the magnification for each off-axis image is

$$M_{\rm off} = -\frac{\gamma}{(1+\gamma)A} \tag{27}$$

where $A \equiv 4\gamma^2 - (1+\gamma)\zeta^2$. If $\lvert\zeta\rvert < 2\gamma(1+\gamma)^{-1/2}$, this is negative so that both off-axis images are of negative parity. If $\lvert\zeta\rvert = 2\gamma(1+\gamma)^{-1/2}$, the magnification diverges, implying that $\zeta = \pm 2\gamma(1+\gamma)^{-1/2}$ are the caustic points along the real axis. The resulting expressions for the magnifications of the on-axis images are rather complicated, but their sum, product, and difference, which can be derived using resultant quadratic polynomials, are simpler to write down;

$$\begin{aligned} &M_1 + M_2 = -\frac{\zeta^2 - 2\gamma}{(1-\gamma)A}\,; \qquad M_1 M_2 = \frac{1}{(1-\gamma)AB}\,; \\ &|M_1 - M_2| = \frac{|\zeta||\zeta^2 - 4\gamma + 2|}{|1-\gamma||A|\sqrt{B}}, \end{aligned} \tag{28}$$

where $B \equiv \zeta^2 + 4(1-\gamma)$ as defined following equation (26). With $B > 0$, the two on-axis images are of the same parity if $(1-\gamma)A > 0$, whereas they are of opposite parity if $(1-\gamma)A < 0$. In particular, if $0 \leqslant \gamma < 1$ and $\lvert\zeta\rvert < 2\gamma(1+\gamma)^{-1/2}$, both are positive parity images, whilst both are negative parity images if $\gamma > 1$ and $\lvert\zeta\rvert > 2\gamma(1+\gamma)^{-1/2}$. Again, if $\zeta = \pm 2\sqrt{\gamma-1}$ with $\gamma > 1$ or if $\zeta = \pm 2\gamma(1+\gamma)^{-1/2}$, the magnification of either of the on-axis images diverges, so that the source location corresponds to the caustic point. The total magnification can be found from the sum of the absolute values of the individual magnifications corresponding to the actual image positions. The results for all these case are summarized in Table 1. We find that two negative off-axis images and one positive on-axis image merge into one negative on-axis image at $\zeta = \pm 2\gamma(\gamma+1)^{-1/2}$, whereas two opposite parity on-axis images appear or disappear simply by merging with each other at $\zeta = \pm 2\sqrt{\gamma-1}$. Note that this reflects that the formers are actually cusp points while the latters are simple first-order caustic points.

4.2 The Imaginary Axis

The lensing of the source along the imaginary axis (i.e., $\bar{\zeta} = -\zeta$) can be analyzed in a similar manner. First, by considering the solutions on the imaginary axis ($\bar{z} = -z$), we can easily factor $g_{\rm n}(z)$ into two quadratics if $\bar{\zeta} = -\zeta$ and $\bar{\gamma} = \gamma$, and subsequently find the zeros of $g_{\rm n}(z)$:

$$\begin{aligned} z_{\rm on} &= \mathrm{i}\,\frac{\Im[\zeta] \pm \left[|\zeta|^2 + 4(1+\gamma)\right]^{1/2}}{2(1+\gamma)} \\ z_{\rm off} &= \frac{\mathrm{i}\,\Im[\zeta]}{2\gamma} \pm \frac{1}{2\gamma}\left(\frac{4\gamma^2}{1-\gamma} - |\zeta|^2\right)^{1/2}. \end{aligned} \tag{29}$$

Here, $\zeta = \mathrm{i}\Im[\zeta]$ with $\Im[\zeta] \in \mathbb{R}$ and $\zeta^2 = -|\zeta|^2 \leqslant 0$. With $\gamma \geqslant 0$, the two on-axis zeros $z_{\rm on}$ are always image positions. On the other hand, the two off-axis zeros $z_{\rm off}$ become image positions if $0 \leqslant \gamma < 1$ and $|\zeta| < 2\gamma(1-\gamma)^{-1/2}$. The two off-axis solutions are related to each other by $z \leftrightarrow -\bar{z}$, which is also a transformation that leaves equation (4) invariant, and so they have identical magnifications too, namely

$$M_{\rm off} = \frac{\gamma}{(1-\gamma)C}, \tag{30}$$

where $C \equiv 4\gamma^2 - (1-\gamma)|\zeta|^2$. We find $M_{\rm off}$ to be positive if $|\zeta| < 2\gamma(1-\gamma)^{-1/2}$ with $0 \leqslant \gamma < 1$. The sum, product, and difference of the two on-axis images are similarly found to be

$$\begin{aligned} &M_1 + M_2 = -\frac{|\zeta|^2 + 2\gamma}{(1+\gamma)C}\,; \qquad M_1 M_2 = \frac{1}{(1+\gamma)CD}\,; \\ &|M_1 - M_2| = \frac{|\zeta|(|\zeta|^2 + 4\gamma + 2)}{(1+\gamma)|C|\sqrt{D}}, \end{aligned} \tag{31}$$

where $D \equiv |\zeta|^2 + 4(1+\gamma)$. This indicates that the two on-axis images are of opposite parity if $C < 0$ and that they are both negative parity images if $C > 0$. Along the imaginary axis, the caustic points occur at $\zeta = \pm 2\mathrm{i}\gamma(1-\gamma)^{-1/2}$ with $0 \leqslant \gamma < 1$, for which two positive off-axis images merges with one negative on-axis image into one positive on-axis image. We provide a summary of these results including the total magnification in Table 2.

We note that the case of the source on the imaginary axis with a positive real shear is actually mathematically identical to the case of the source along the real axis with a *negative* real shear, modulo a 90° rotation of the system. In fact, equations (29-31) can be obtained from equations (26-28) through the transformation $\gamma \to -\gamma$ (and $z \to \mathrm{i}z$). Nonetheless, we chose to present the case when the source lies on the symmetry axis that is perpendicular to the shear separately from that on the axis that is parallel, in order to clarify the physical difference between the two cases.

Table 2. Summary of the image properties for the cases when the source lies on the imaginary axis (perpendicular to the direction of the shear or parallel to the direction of the tide-causing mass). Here, $C = 4\gamma^2 - (1-\gamma)|\zeta|^2 = 4\gamma^2 + (\gamma-1)|\zeta|^2$ and $D = |\zeta|^2 + 4(1+\gamma)$.

Shear	Source Position	Images	Total Magnification $M_{\rm tot}$
$0 \leqslant \gamma < 1$	$\lvert\zeta\rvert < 2\gamma(1-\gamma)^{-1/2}$	4 images [2 on $(-,-)$ & 2 off $(+,+)$]	$\dfrac{4\gamma + (1-\gamma)\lvert\zeta\rvert^2}{(1-\gamma^2)C}$
$0 \leqslant \gamma < 1$	$\lvert\zeta\rvert > 2\gamma(1-\gamma)^{-1/2}$	2 images [2 on $(+,-)$]	$\dfrac{\lvert\zeta\rvert(\lvert\zeta\rvert^2 + 4\gamma + 2)}{(1+\gamma)(-C)\sqrt{D}}$
$\gamma > 1$	any	2 images [2 on $(-,-)$]	$\dfrac{\lvert\zeta\rvert^2 + 2\gamma}{(\gamma+1)C}$

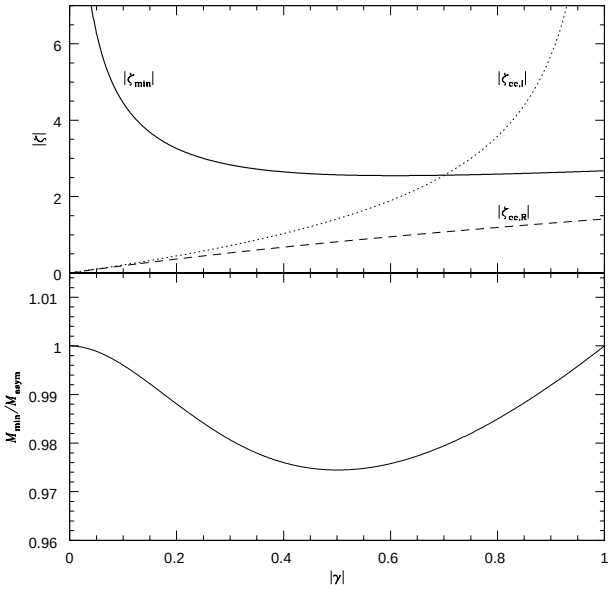

Figure 1. Top: The location of the global minimum magnification for the source on the real axis for $0 \leqslant \gamma < 1$ (solid line). Also plotted are the locations of the caustic points (in fact, cusp points) along the real axis (dashed line) and along the imaginary axis (dotted line). Bottom: The ratio of the global minimum magnification $M_{\rm min}$ to the asymptotic magnification $M_{\rm asym} = (1-\gamma^2)^{-1}$ at infinity.

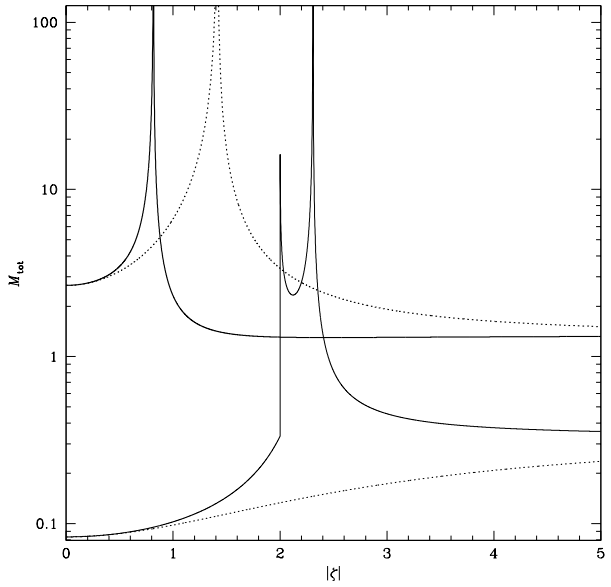

Figure 2. Magnification along the symmetry axis. Thick lines are for $\gamma = 1/2$ while thin lines are for $\gamma = 2$. The solid lines are along the real axis (parallel to the direction of the shear), and the dotted lines are along the imaginary axis (perpendicular to the direction of the shear).

4.3 The Magnification along the Symmetry Axis

For $0 \leqslant \gamma < 1$, the total magnification of the source at the centre is $M_{\rm tot} = [\gamma(1-\gamma^2)]^{-1}$. As the source moves along the symmetry axis, the magnification increases until the source crosses the caustics where the magnification diverges. The caustic points on the real axis are located at $\zeta = \pm 2\gamma(1+\gamma)^{-1/2}$, while the ones on the imaginary axis are at $\zeta = \pm 2{\rm i}\gamma(1-\gamma)^{-1/2}$. So, we deduce that the caustic is elongated along the imaginary axis (i.e., perpendicular to the shear direction or parallel to the direction of the tide-causing mass). The magnification initially decreases from infinity as the source moves past the caustic points along the symmetry axis. Along the imaginary axis, it decreases monotonically and tends to $(1-\gamma^2)^{-1}$ at infinity. Along the real axis, however, the global minimum magnification, which is slightly smaller than the asymptotic magnification, occurs at some finite distance from the centre, and the magnification increases back to the asymptotic value $(1-\gamma^2)^{-1}$ at infinity. The location and the value of the global minimum magnification (as a function of γ) can in principle be derived from the expression for the total magnification given in Table 1;

$$\zeta_{\rm min}^2 = 4\gamma - 1 + \frac{1+E}{\gamma}\,; \qquad E = \sqrt{1 - 2\gamma + 9\gamma^2}$$

$$M_{\rm min} = \frac{1+\gamma+E}{(1-\gamma)[1+3\gamma^2+(1+\gamma)E]}\sqrt{\frac{1-\gamma+4\gamma^2+E}{1+3\gamma+E}}. \qquad (32)$$

Figure 1 shows $|\zeta_{\rm min}|$ and $M_{\rm min}/M_{\rm asym}$ as functions of γ where $M_{\rm asym} = (1-\gamma^2)^{-1}$ is the asymptotic magnification. We find that $M_{\rm min} > 1$ and that $M_{\rm min} \approx M_{\rm asym}$. In fact, for $0 < \gamma < 1$, we have $1 > M_{\rm min}/M_{\rm asym} \geqslant 9\sqrt{3}/16 \approx 0.97428$ where the minimum of $M_{\rm min}/M_{\rm asym}$ occurs at $\gamma = 1/2$. In Fig. 2, we plot the behaviour of the total magnification, as the source moves along the symmetry axis for $\gamma = 1/2$.

For $\gamma > 1$, the total magnification for the source at the centre is given by $[2\gamma(\gamma+1)]^{-1}$ (which is actually the global minimum magnification), so that the lensed images are in fact demagnified compared to the source. The magnification increases as the source moves along the symmetry axis. Along the imaginary axis, the magnification monotonically increases throughout and tends to the asymptotic value $(\gamma^2-1)^{-1}$ at infinity. Along the real axis, there is a discontinuous jump in the magnification to infinity when the source crosses the caustic at $\zeta = \pm 2\sqrt{\gamma-1}$. As the source moves across the caustic, the magnification drops from infinity to a lo-

cal minimum value and then diverges back to infinity as the source approaches the other caustic points $\zeta = \pm 2\gamma(\gamma+1)^{-1/2}$ along the real axis. Once the source moves out of the caustic, the magnification monotonically decreases from infinity and tends to the same asymptotic value $(\gamma^2-1)^{-1}$. Here, the local minimum value of the magnification and the corresponding source position within the caustic are actually easy to find. First, we note that there are four images – one positive and three negative parity – for the case considered here. However, from the signed magnification sum invariant given in equation (20), we find that the total magnification is completely specified by the magnification M_+ of the positive parity image alone, that is, $M_{\rm tot} = 2M_+ - (1-\gamma^2)^{-1}$. Finally, from equation (4), the minimum possible magnification of any positive parity image is unity when $z^2 = \overline{\gamma}^{-1}$. With $\overline{\gamma} = \gamma > 1$, we find that $z = \pm\gamma^{-1/2}$ maps to $\zeta = \mp\gamma^{-1/2}(2\gamma-1)$ so that we in fact have $2\sqrt{\gamma-1} < |\zeta| < 2\gamma(\gamma+1)^{-1/2}$ and the corresponding local minimum magnification is given by $M_{\rm tot} = (2\gamma^2-1)/(\gamma^2-1)$. In Fig. 2, we also plot the total magnification for the source on the symmetry axis for $\gamma = 2$.

5 CRITICAL CURVES AND CAUSTICS

From equation (4), the parametric representation of the critical curve can be found (Witt 1990) by solving

$$\frac{1}{z_{\rm c}^2} - \overline{\gamma} = {\rm e}^{-2{\rm i}\phi} \qquad \rightarrow \qquad z_{\rm c}^2 = \frac{1}{\overline{\gamma}+{\rm e}^{-2{\rm i}\phi}} = \frac{{\rm e}^{2{\rm i}\phi}}{1+\overline{\gamma}{\rm e}^{2{\rm i}\phi}}. \tag{33}$$

Here, the closed form solutions for the critical curve involve the square-root, but because of the presence of the branch-cut in the mapping of $z^{1/2}$, we need to be careful. Once the branch-cut of the mapping $z^{1/2}$ is assumed to lie along the negative real axis, the resulting expressions for the critical curve and the caustic should differ depending on the magnitude of $|\gamma|$ in order to avoid crossing the branch-cut (i.e., there is no discontinuous jump in the resulting parametric expression). Hence, we find the parametric representations of the critical curves

$$z_{\rm c}(\phi) = \frac{{\rm e}^{{\rm i}\phi}}{(1+\overline{\gamma}{\rm e}^{2{\rm i}\phi})^{1/2}} = \frac{{\rm e}^{{\rm i}\tilde{\phi}}}{\left(1+|\gamma|{\rm e}^{2{\rm i}\tilde{\phi}}\right)^{1/2}}\,{\rm e}^{{\rm i}\phi_\gamma} \tag{34}$$

for $0 \leqslant |\gamma| < 1$, and

$$z_{\rm c}(\phi) = \pm\frac{1}{\overline{\gamma}^{1/2}\,(1+\overline{\gamma}^{-1}{\rm e}^{-2{\rm i}\phi})^{1/2}} = \pm\frac{1}{\left(|\gamma|+{\rm e}^{-2{\rm i}\tilde{\phi}}\right)^{1/2}}\,{\rm e}^{{\rm i}\phi_\gamma} \tag{35}$$

for $|\gamma| > 1$. Here, $\gamma = |\gamma|{\rm e}^{2{\rm i}\phi_\gamma}$ and $\tilde{\phi} = \phi - \phi_\gamma$. The parametric representation of the caustics can be found by mapping the critical curve though the lens equation (2);

$$\zeta_{\rm c}(\phi) = z_{\rm c}(\phi) - \frac{1}{\overline{z}_{\rm c}(\phi)} - \gamma\overline{z}_{\rm c}(\phi). \tag{36}$$

However, before we actually derive expressions, let us examine first

$$\begin{aligned}\zeta_{\rm c}'(\phi) &= z_{\rm c}'(\phi)\partial_z\zeta + \overline{z}_{\rm c}'(\phi)\partial_{\overline{z}}\zeta = z_{\rm c}'(\phi) + {\rm e}^{2{\rm i}\phi}\overline{z}_{\rm c}'(\phi)\\ &= {\rm e}^{{\rm i}\phi}\left[{\rm e}^{-{\rm i}\phi}z_{\rm c}'(\phi) + {\rm e}^{{\rm i}\phi}\overline{z}_{\rm c}'(\phi)\right] = 2{\rm e}^{{\rm i}\phi}\Re[{\rm e}^{-{\rm i}\phi}z_{\rm c}'(\phi)].\end{aligned} \tag{37}$$

In other words, we find that $\zeta_{\rm c}'(\phi)$ is parallel to ${\rm e}^{{\rm i}\phi}$, that is, the parameter ϕ is defined such that it is the argument angle of the tangent to the caustics at the caustic point. Furthermore, we also find that the caustics form a cusp point [$\zeta_{\rm c}'(\phi) = 0$] if ${\rm e}^{-{\rm i}\phi}z_{\rm c}'(\phi)$ is pure imaginary number, that is $z_{\rm c}'(\phi) = {\rm i}r{\rm e}^{{\rm i}\phi}$ with $r \in \mathbb{R}$. This indicates that $z_{\rm c}'(\phi)$ is orthogonal to ${\rm e}^{{\rm i}\phi}$ at the critical point corresponding to a cusp point. In fact, the general condition for the cusp along the caustics is that the tangent to the caustic is the normal direction to the critical curve at the corresponding caustic point and the critical point.

Now, the actual parametric expression of the caustics of the Chang–Refsdal lens are given by

$$\begin{aligned}\zeta_{\rm c}(\phi) &= {\rm e}^{{\rm i}\phi}\left[\frac{1}{(1+\overline{\gamma}{\rm e}^{2{\rm i}\phi})^{1/2}} - \frac{1+2\gamma{\rm e}^{-2{\rm i}\phi}}{(1+\gamma{\rm e}^{-2{\rm i}\phi})^{1/2}}\right]\\ &= {\rm e}^{{\rm i}\tilde{\phi}}\left[\frac{1}{\left(1+|\gamma|{\rm e}^{2{\rm i}\tilde{\phi}}\right)^{1/2}} - \frac{1+2|\gamma|{\rm e}^{-2{\rm i}\tilde{\phi}}}{\left(1+|\gamma|{\rm e}^{-2{\rm i}\tilde{\phi}}\right)^{1/2}}\right]{\rm e}^{{\rm i}\phi_\gamma}\end{aligned} \tag{38}$$

for $0 \leqslant |\gamma| < 1$, and

$$\begin{aligned}\zeta_{\rm c}(\phi) &= \pm\frac{1}{\overline{\gamma}^{1/2}}\left[\frac{1}{(1+\overline{\gamma}^{-1}{\rm e}^{-2{\rm i}\phi})^{1/2}} - |\gamma|\frac{2+\gamma^{-1}{\rm e}^{2{\rm i}\phi}}{(1+\gamma^{-1}{\rm e}^{2{\rm i}\phi})^{1/2}}\right]\\ &= \pm\left[\frac{1}{\left(|\gamma|+{\rm e}^{-2{\rm i}\tilde{\phi}}\right)^{1/2}} - \frac{2|\gamma|+{\rm e}^{2{\rm i}\tilde{\phi}}}{\left(|\gamma|+{\rm e}^{2{\rm i}\tilde{\phi}}\right)^{1/2}}\right]{\rm e}^{{\rm i}\phi_\gamma}\end{aligned} \tag{39}$$

for $|\gamma| > 1$. Here, we note that the critical curves and the caustics are single simply-connected curves with $\phi \in [0, 2\pi)$ for $0 \leqslant |\gamma| < 1$, while they are two separate mirror-symmetric closed curves with $\phi \in [0, \pi)$ for $\gamma > 1$.

The cusp points along the caustics can be found using

$$\zeta_{\rm c}'(\phi) = 2{\rm e}^{{\rm i}\phi}\Im\left[\frac{1}{(1+\gamma{\rm e}^{-2{\rm i}\phi})^{3/2}}\right] \tag{40}$$

for $0 \leqslant |\gamma| < 1$, and

$$\zeta_{\rm c}'(\phi) = \pm 2{\rm e}^{{\rm i}\phi}\Im\left[\frac{{\rm e}^{3{\rm i}\phi}}{(\gamma+{\rm e}^{2{\rm i}\phi})^{3/2}}\right] \tag{41}$$

for $|\gamma| > 1$. First, for $0 \leqslant |\gamma| < 1$, we find that the condition $\zeta_{\rm c}'(\phi) = 0$ is equivalent to $(1+|\gamma|{\rm e}^{2{\rm i}\tilde{\phi}})^{3/2} \in \mathbb{R}$ so that we have $2{\rm i}\tilde{\phi} = n\pi$ for $\tilde{\phi}$ corresponding to the cusp points. Here, n is an integer. Hence, the caustics have four cusps at

$$\zeta_{\rm cc} = \pm{\rm e}^{{\rm i}\phi_\gamma}\frac{2|\gamma|}{(1+|\gamma|)^{1/2}}\,; \qquad \zeta_{\rm cc} = \pm{\rm i}{\rm e}^{{\rm i}\phi_\gamma}\frac{2|\gamma|}{(1-|\gamma|)^{1/2}}, \tag{42}$$

which is consistent with the result in the previous section. Next, for $|\gamma| > 1$, the condition that $\zeta_{\rm c}'(\phi) = 0$ reduces to $\left(|\gamma|{\rm e}^{2{\rm i}\tilde{\phi}}+1\right)^3$ being a *positive* real number, or equivalently $\arg(1+|\gamma|{\rm e}^{2{\rm i}\tilde{\phi}}) = (2n\pi)/3$ where n is again an integer. From simple geometric considerations, this reduces to $2\tilde{\phi} = 2n\pi$, $2n\pi + (2\pi)/3 + \xi$, or $2n\pi + (4\pi)/3 - \xi$ where $\xi = \arcsin[\sqrt{3}/(2|\gamma|)]$. Therefore, we find that there are three cusps along each caustic (hence, in total six, $2\times 3 = 6$) at

$$\begin{aligned}\zeta_{\rm cc} &= \pm{\rm e}^{{\rm i}\phi_\gamma}\frac{\sqrt{2}{\rm e}^{{\rm i}\xi/2}}{\left(\sqrt{4|\gamma|^2-3}-1\right)^{1/2}}\left(2-\sqrt{4|\gamma|^2-3}+{\rm e}^{2{\rm i}\pi/3}\right)\\ \zeta_{\rm cc} &= \pm{\rm e}^{{\rm i}\phi_\gamma}\frac{\sqrt{2}{\rm e}^{-{\rm i}\xi/2}}{\left(\sqrt{4|\gamma|^2-3}-1\right)^{1/2}}\left(2-\sqrt{4|\gamma|^2-3}+{\rm e}^{-2{\rm i}\pi/3}\right)\\ \zeta_{\rm cc} &= \mp{\rm e}^{{\rm i}\phi_\gamma}\frac{2|\gamma|^{1/2}}{(1+|\gamma|^{-1})^{1/2}}.\end{aligned} \tag{43}$$

5.1 The Areas under the Critical Curves and the Caustics

Next, since ${\rm e}^{2{\rm i}\phi}$ is periodic for ϕ (with period π), one can conclude that $z_{\rm c}(\phi)$ [and consequently $\zeta_{\rm c}(\phi)$] is also periodic although the period is not necessarily π. If there exists a convergent Fourier-series expansion

$$z_{\rm c}(\phi) = \sum_{k=-\infty}^{\infty} c_k{\rm e}^{{\rm i}k\omega\phi}\,; \qquad \zeta_{\rm c}(\phi) = \sum_{k=-\infty}^{\infty} d_k{\rm e}^{{\rm i}k\omega\phi} \tag{44}$$

where ω is the angular frequency of $z_c(\phi)$ [i.e., the ϕ-period of $z_c(\phi)$ is $2\pi/\omega$], then from

$$\zeta_c'(\phi) = z_c'(\phi) + e^{2i\phi}\overline{z}_c'(\phi) = \sum_k ik\omega c_k e^{ik\omega\phi} - \sum_k ik\omega\overline{c}_k e^{i(2-k\omega)\phi}$$
$$= \sum_k i\omega\left[kc_k + \left(k - \frac{2}{\omega}\right)\overline{c}_{2/\omega-k}\right]e^{ik\omega\phi}, \quad (45)$$

we find that $kd_k = kc_k + (k-2/\omega)\overline{c}_{2/\omega-k}$, assuming $2/\omega$ is an integer [i.e, the ϕ-period of $z_c(\phi)$ is an integer multiple of π]. Here, the relations for $k = 0$ and $k = 2/\omega$ together indicate that $c_{2/\omega} = d_{2/\omega} = 0$, whereas c_0 and d_0 are unspecified. Then the caustics may be written in terms of c_k's as

$$\zeta_c(\phi) - d_0 = \sum_{k\neq 0}\left[c_k + \frac{k-2/\omega}{k}\overline{c}_{2/\omega-k}\right]e^{ik\omega\phi}$$
$$= \sum_{k\neq 2/\omega}\frac{(k-2/\omega)c_k e^{ik\omega\phi} + k\overline{c}_k e^{-i(k\omega-2)\phi}}{k-2/\omega} - c_0. \quad (46)$$

One application for which the Fourier-series expansions may be useful is to find the area within the critical curve and the caustics. We note that the 'area 2-form' in $\mathbb{C}$ may be written as $d^2\boldsymbol{x} = d(\overline{z}dz)/(2i)$.[3] Then, the (signed) area within a simply-connected closed curve $\partial C = \{z(p)|z(p) : [0, P) \to \mathbb{C}, p \in [0, P) \subset \mathbb{R}\}$ where p is a parameter and P is the period can be found to be, from the fundamental theorem of multivariate calculus – the 'generalized Stoke's theorem' (c.f., Gould & Gaucherel 1997; Dominik 1998)

$$S = \int_C d^2\mathbf{x} = \frac{1}{2i}\int_C d(\overline{z}dz) = \frac{1}{2i}\oint_{\partial C}\overline{z}\,dz = \frac{1}{2i}\int_0^P \overline{z}(p)\,z'(p)\,dp. \quad (47)$$

The area within the critical curve can be expressed in terms of its Fourier coefficients, from the generalized Parseval's theorem, as

$$S[z(\phi)] = \frac{1}{2i}\int_0^{2\pi/\omega}\overline{z}_c(\phi)\,z_c'(\phi)\,d\phi = \pi\sum_k k|c_k|^2. \quad (48)$$

Provided (i) that the period of $\zeta_c(\phi)$ is also $2\pi/\omega$ and (ii) that the caustic $\zeta_c(\phi)$ does not exhibit self-intersection, the area within the caustic can also be written in similar manner

$$\frac{S[\zeta_c(\phi)]}{\pi} = \sum_k k|d_k|^2 = \sum_{k\neq 0}\frac{1}{k}\left|kc_k + \left(k-\frac{2}{\omega}\right)\overline{c}_{2/\omega-k}\right|^2$$
$$= \sum_{k\neq 2/\omega}\frac{2k}{2-k\omega}|c_k|^2 - \frac{2}{\omega}\sum_k \Re[c_k c_{2/\omega-k}]. \quad (49)$$

We note that this is typically negative as the orientation chosen by the parameter ϕ is usually clockwise.

For $0 \leqslant |\gamma| < 1$, from equation (34), we find the Fourier-series expansions of the critical curves and the caustics to be

$$z_c e^{-i\phi_\gamma} = \sum_{k=0}^{\infty}\frac{(-1)^k}{k!}\left(\frac{1}{2}\right)_k |\gamma|^k e^{(2k+1)i\tilde{\phi}} \quad (50)$$

$$\zeta_c e^{-i\phi_\gamma} = \sum_{k=1}^{\infty}\frac{C_k}{2}\left[(2k-1)e^{(2k+1)i\tilde{\phi}} + (2k+1)e^{-(2k-1)i\tilde{\phi}}\right]|\gamma|^k \quad (51)$$

where $(a)_k$ is Pochhammer symbol such that

$$(a)_k \equiv a(a+1)\cdots(a+k-1) = \frac{\Gamma(a+k)}{\Gamma(a)} \quad (52)$$

[3] $d(\overline{z}dz) = d\overline{z}\wedge dz = (dx_1 - i\,dx_2)\wedge(dx_1 + i\,dx_2) = 2i\,dx_1\wedge dx_2$

and

$$C_k = (-1)^k\frac{\Gamma(k-1/2)}{k!\Gamma(1/2)}. \quad (53)$$

We note that both series expansions are also Taylor-series expansions with respect to γ at $\gamma = 0$. If we truncate the expansion of the caustic after $(k = 1)$-term, the expression reduces to the equation of the tetra-cuspi-hypocycloid, or the astroid. The fact that the caustic for the Chang–Refsdal lens with $0 \leqslant |\gamma| < 1$ has an astroid-like shape has been widely acknowledged. In fact, the astroid is the generic shape of the caustic for a lens system under a weak quadrupole perturbation (Kovner 1987; An 2005). Here, the ϕ-period of both curves are 2π, and both are simply connected. Thus, the area under each curve is

$$S[z_c] = \sum_{k=0}^{\infty}\frac{2\Gamma(k+1/2)\Gamma(k+3/2)}{\Gamma(k+1)^2}|\gamma|^{2k}$$
$$= \pi\,{}_2F_1\left(\frac{1}{2},\frac{3}{2};1;|\gamma|^2\right) \quad (54)$$

$$S[\zeta_c] = \sum_{k=0}^{\infty}\frac{2\Gamma(k+1/2)\Gamma(k+5/2)}{\Gamma(k+2)^2}|\gamma|^{2k+2}$$
$$= 2\pi\left[1 - {}_2F_1\left(-\frac{1}{2},\frac{3}{2};1;|\gamma|^2\right)\right] \quad (55)$$

where ${}_2F_1(a, b; c; x)$ is the Gaussian hypergeometric function. The result for the area under the caustics expressed using the elliptic integrals (see Appendix A) can be compared to the area under the planetary caustics due to an 'external' planet (see e.g. Bozza 2000), which is basically in the same form up to the overall scale factor ($\propto q$) once $|\gamma| \propto d^{-2}$ has been properly chosen, where q and d are the mass ratio and the separation in units of Einstein ring of the planetary companion. This is because the effect of the primary star on microlensing due to the planet can be well approximated by the Chang–Refsdal lens (Gould & Loeb 1992; Gaudi & Gould 1997; Bozza 1999). This is also the case for any point mass lens perturbed by mass lying far outside of its Einstein ring radius, as in a wide-separation binary for instance (Dominik 1999; Bozza 2000; An 2005).

For $|\gamma| > 1$, we find the Fourier-series expansion of the critical curve as

$$z_c e^{-i\phi_\gamma} = \pm\frac{1}{|\gamma|^{1/2}}\left\{1 + \sum_{k=1}^{\infty}\frac{(-1)^k}{k!}\left(\frac{1}{2}\right)_k\frac{e^{-2ki\tilde{\phi}}}{|\gamma|^k}\right\} \quad (56)$$

and the caustic

$$\zeta_c e^{-i\phi_\gamma} = \mp|\gamma|^{1/2}\left\{\tilde{d}_0 + \sum_{k=2}^{\infty}C_k\frac{(k-1)e^{2ki\tilde{\phi}} + ke^{-2(k-1)i\tilde{\phi}}}{|\gamma|^k}\right\}. \quad (57)$$

where C_k is given by equation (53) and

$$\tilde{d}_0 = 2 - \frac{1}{|\gamma|}. \quad (58)$$

Unlike the previous case, the leading terms are given by a constant. Hence, we find that the critical curves are 'centred' at $z = \pm|\gamma|^{-1/2}e^{i\phi_\gamma}$, and that the caustics are at $\zeta = \pm(|\gamma|^{-1/2} - 2|\gamma|^{1/2})e^{i\phi_\gamma}$. The truncation of the series for the caustic after the first non-constant term for this case leads to the equation of the tri-cuspi-hypocycloid, or the deltoid. In other words, as $|\gamma| \to \infty$, the caustics reduce to a pair of mirror-symmetric deltoids. Here, the ϕ-period of each separate curve is given by π so that the area under each is

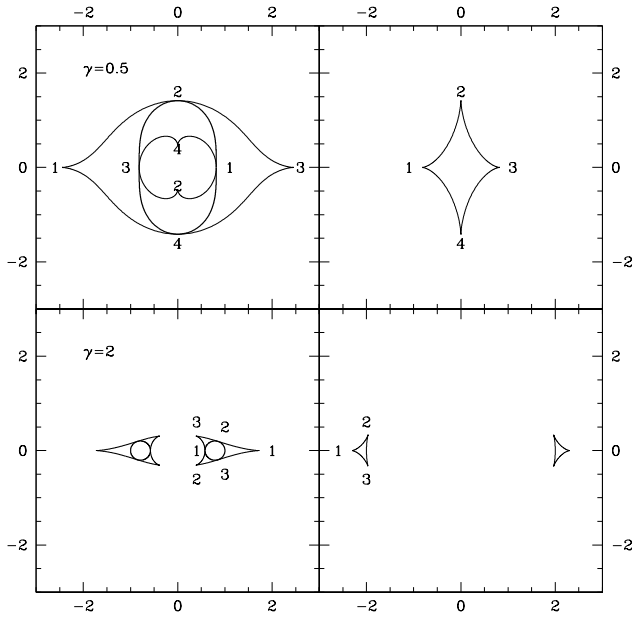

Figure 3. Critical curves, pre-caustics, and caustics of the Chang–Refsdal lens. The top panels are for $\gamma = 1/2$ and the bottom panels are for $\gamma = 2$. The left panels show the critical curves (thick lines) and the pre-caustics (thin lines), and the right panels show the caustics. The numbers indicate corresponding points mapped under the lens mapping.

found to be

$$S[z_c] = \sum_{k=0}^{\infty} \frac{\Gamma(k+3/2)^2}{\Gamma(k+1)\Gamma(k+2)} \frac{1}{|\gamma|^{2k+3}} = \frac{\pi}{4|\gamma|^3}\, {}_2F_1\left(\frac{3}{2},\frac{3}{2};2;\frac{1}{|\gamma|^2}\right) \quad (59)$$

$$S[\zeta_c] = \sum_{k=0}^{\infty} \frac{\Gamma(k+3/2)^2}{\Gamma(k+1)\Gamma(k+3)} \frac{1}{|\gamma|^{2k+3}} = \frac{\pi}{8|\gamma|^3}\, {}_2F_1\left(\frac{3}{2},\frac{3}{2};3;\frac{1}{|\gamma|^2}\right) \quad (60)$$

Here, the area derived is for each one of the curves, and therefore, the total area under the critical curves and the caustics is twice this result. Again, the results expressed in terms of elliptic integrals are provided in Appendix A.

5.2 Pre-caustics

Since the critical points are the degenerate zeros of the imaging polynomial corresponding to the source on a caustic point, the corresponding pre-caustic points can be found from the remaining zeros of the polynomial after the two degenerate linear factors $(z-z_c)^2$ have been factored out. The coefficients of the resulting quadratic polynomials $p_2 z^2 + p_1 z + p_0$ are (for simplicity, γ is taken to be real)

$$\begin{aligned} p_2 &= \gamma(1-\gamma^2)\,; \\ p_1 &= \mathrm{e}^{-\mathrm{i}\phi}\left[\frac{1+\gamma\mathrm{e}^{2\mathrm{i}\phi}}{(1+\gamma\mathrm{e}^{-2\mathrm{i}\phi})^{1/2}} - (1-2\gamma^2)\left(1+\gamma\mathrm{e}^{2\mathrm{i}\phi}\right)^{1/2}\right]; \\ p_0 &= -\gamma\mathrm{e}^{-2\mathrm{i}\phi}(1+\gamma\mathrm{e}^{2\mathrm{i}\phi}) \end{aligned} \quad (61)$$

for $0 \leqslant \gamma < 1$, and

$$\begin{aligned} p_2 &= \gamma(\gamma^2-1)\,; \\ p_1 &= \mp\left[(2\gamma^2-1)\left(\gamma+\mathrm{e}^{-2\mathrm{i}\phi}\right)^{1/2} + \frac{1+\gamma\mathrm{e}^{2\mathrm{i}\phi}}{(\gamma+\mathrm{e}^{2\mathrm{i}\phi})^{1/2}}\right]; \\ p_0 &= \gamma(\gamma+\mathrm{e}^{-2\mathrm{i}\phi}) \end{aligned} \quad (62)$$

for $\gamma > 1$. Finally, we find the parametric expression of the pre-caustics to be

$$z_p^+ = \mathrm{e}^{-\mathrm{i}\phi}\frac{\left(1+\gamma\mathrm{e}^{2\mathrm{i}\phi}\right)^{1/2}}{2\gamma(1-\gamma^2)}\left[1-2\gamma^2-\frac{\left(1+\gamma\mathrm{e}^{2\mathrm{i}\phi}\right)^{1/2}+r}{(1+\gamma\mathrm{e}^{-2\mathrm{i}\phi})^{1/2}}\right] \quad (63)$$

$$z_p^- = \mathrm{e}^{-\mathrm{i}\phi}\frac{\left(1+\gamma\mathrm{e}^{2\mathrm{i}\phi}\right)^{1/2}}{2\gamma(1-\gamma^2)}\left[1-2\gamma^2-\frac{\left(1+\gamma\mathrm{e}^{2\mathrm{i}\phi}\right)^{1/2}-r}{(1+\gamma\mathrm{e}^{-2\mathrm{i}\phi})^{1/2}}\right] \quad (64)$$

for $0 \leqslant \gamma < 1$, and

$$z_p = \pm\frac{\left(\gamma+\mathrm{e}^{-2\mathrm{i}\phi}\right)^{1/2}}{2\gamma(\gamma^2-1)}\left[2\gamma^2-1+\frac{\left(\gamma+\mathrm{e}^{-2\mathrm{i}\phi}\right)^{1/2}\mathrm{e}^{2\mathrm{i}\phi}+r\mathrm{e}^{\mathrm{i}\phi}}{(\gamma+\mathrm{e}^{2\mathrm{i}\phi})^{1/2}}\right] \quad (65)$$

for $\gamma > 1$. Here,

$$\frac{r^2}{2} = 1+\gamma\cos 2\phi - (1-2\gamma^2)\left(1+\gamma^2+2\gamma\cos 2\phi\right)^{1/2}. \quad (66)$$

We note that, for $0 \leqslant \gamma < 1$, the pre-caustics are two separate curves, one of which $z_p^+(\phi)$ completely encloses the critical curve and the other of which $z_p^-(\phi)$ is completely enclosed by the critical curve. We also find that the curve $z_p^-(\phi)$ is in the generic shape of the bi-cuspi-epicycloid, or the nephroid whereas $z_p^+(\phi)$, as a whole, appears to be the inverse curve of $z_p^-(\phi)$ with respect to the origin, rotated by 90° and rescaled by a factor of $\sqrt{1-\gamma^2}$. On the other hand, for $\gamma > 1$, the pre-caustics are two mirror-symmetric curves, each of which encloses one of the mirror symmetric critical curves. For both cases, the critical curves and the pre-caustics are co-tangent to one another at the critical points corresponding to the cusp points. The examples for $\gamma = 1/2$ and $\gamma = 2$ are shown in Fig. 3.

Following Finch et al. (2002), the ratio of the areas under the caustics and the pre-caustics provides us with the mean total magnification of the source that lies within the caustic. Although the complicated parametric forms of the pre-caustics indicate that the analytic evaluation of the area under them using the present expression is tough, following equation (47), it reduces to a one-dimensional (complex-contour) integral, which is straightforward to evaluate numerically. In fact, it turns out that the area under the pre-caustics can be evaluated analytically. The result for $\gamma > 1$ is particularly notable and is given in the next section. On the other hand, the result for $0 \leqslant \gamma < 1$ is more complicated and is simply quoted in Appendix C.

It is known that the asymptotic form of the magnification distribution is given by $P(M) \sim M^{-3}$ if the effect of the divergent magnification in the vicinity of the caustics is dominant (Schneider 1987). If the full magnification distribution for the source in the caustics is well approximated by its asymptotic form $P(M) \sim M^{-3}$ down to the minimum possible value $M^{\rm c}_{\rm min}$, the mean magnification is given by $\langle M\rangle = 2M^{\rm c}_{\rm min}$. Here, $M^{\rm c}_{\rm min} = [\gamma(1-\gamma^2)]^{-1}$ for $0 \leqslant \gamma < 1$ and $M^{\rm c}_{\rm min} = (2\gamma^2-1)/(\gamma^2-1)$ for $\gamma > 1$. In Fig. 4, we plot $\langle M\rangle$ and $\langle M\rangle/M^{\rm c}_{\rm min}$ as a function of $|\gamma|$ to examine how much the magnification distribution deviates from its asymptotic form. Also plotted in Fig. 5 are the effective power-index $n_{\rm eff}$ for the magnification distribution defined such that $\langle M\rangle = [(n_{\rm eff}-1)/(n_{\rm eff}-2)]M^{\rm c}_{\rm min}$, which would be the mean magnification if the magnification distribution were characterized by the power-law $P \propto M^{-n_{\rm eff}}$, and the effective

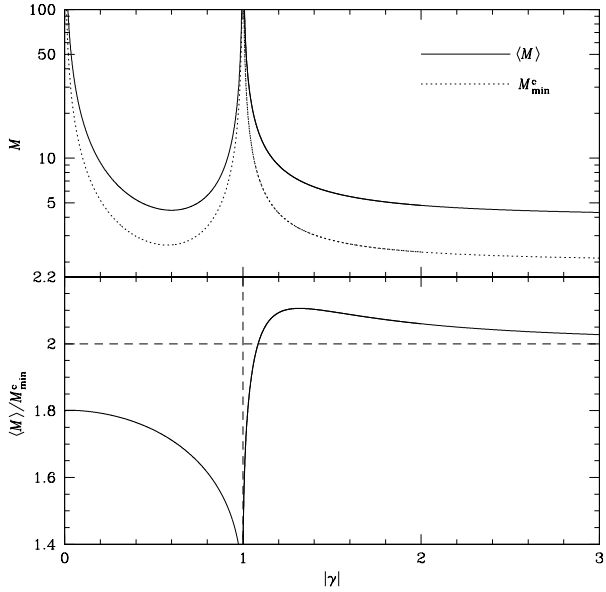

Figure 4. Top: the mean total magnifications $\langle M\rangle$ for the source within the caustic, that is, when there are four images, as a function of $|\gamma|$. Also shown as a dotted line is the minimum possible magnification $M^{\rm c}_{\rm min}$ for the same configuration (that is, 4-image system). Bottom: the ratio $\langle M\rangle/M^{\rm c}_{\rm min}$. The horizontal dashed line marks the ratio of 2, which corresponds to the case that the magnification distribution is given by a truncated power law $P \propto M^{-3}$.

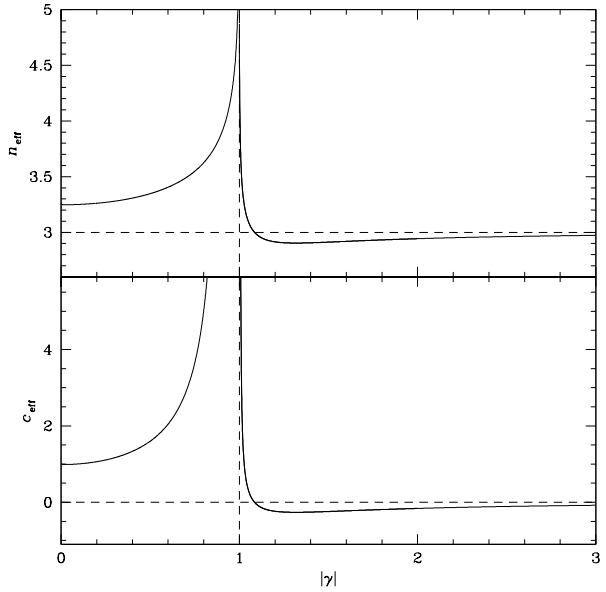

Figure 5. Top: the effective power-index $n_{\rm eff}$ for the magnification distribution. Bottom: the effective fourth-order coefficient $c_{\rm eff}$ in the magnification distribution as a function of $|\gamma|$. See the text for details.

4th-order coefficient $c_{\rm eff}$ for the magnification distribution given from $\langle M\rangle = [3(2+c_{\rm eff})/(3+2c_{\rm eff})]M^{\rm c}_{\rm min}$, which would be the mean magnification if the magnification distribution were characterized by $P(M) \propto M^{-3}(1+c_{\rm eff}M^{\rm c}_{\rm min}/M)$ (note that $1.5M^{\rm c}_{\rm min} < \langle M\rangle \leqslant 3M^{\rm c}_{\rm min}$ for $c_{\rm eff} \geqslant -1$, that is $P(M)$ being non-negative). We find that, for $|\gamma| \gtrsim 1.1$, $\langle M\rangle/M^{\rm c}_{\rm min} \approx 2$ within 5%, implying that $P(M) \sim M^{-3}$ may indeed be a good approximation for the magnification distribution for the source within the deltoid-like caustics down to the minimum possible magnification. In fact, we find the full analytic expression for the magnification distribution for this case in section 6 and show that it is well approximated by $P(M) \sim M^{-3}$. On the other hand, for $0 \leqslant |\gamma| < 1$, $\langle M\rangle/M^{\rm c}_{\rm min}$ is smaller than 2, which implies that the power-law index should be steeper than -3 if the distribution were a truncated power-law, or that there is a significant positive higher order term if $P(M)$ is approximated by a power-series to M with the leading term as $M \to \infty$ given by $\propto M^{-3}$. We also note that the limiting value of $\langle M\rangle/M^{\rm c}_{\rm min}$ as $\gamma \to 0$ is found to be $8(3\pi)^{-1}[3\mathbf{K}(1/2) - 2\mathbf{E}(1/2)] \approx 1.80149$, which translates to approximately $c_{\rm eff} \approx 1$. Here, $\mathbf{K}(x)$ and $\mathbf{E}(x)$ are complete elliptic integrals of the first and second kind (see Appendix A for the notation).

6 LINES OF EQUAL INDIVIDUAL MAGNIFICATION

From equations (4) and (33), it is not only the critical curves but also the lines of equal magnification for an individual image that can be written parametrically. That is, the solution of

$$\frac{1}{z_m^2} - \bar{\gamma} = m\mathrm{e}^{-2\mathrm{i}\phi} \tag{67}$$

defines the locus of image positions for which the magnification is given by $|1-m^2|^2$. The area under each curve is proportional to the cumulative probability that a given image is at least magnified by $|1-m^2|^2$, and thus, its derivative with respect to m is related to the magnification distribution for a given image. Although this is not the distribution of the total magnification for a given source position that we want, it is still of some interest to examine this distribution.

As before, we examine different ranges of $|\gamma|$ separately, but now the dividing line occurs at $|\gamma| = m$ in the general case. First, we consider the case that $0 \leqslant |\gamma| \leqslant m$. For this case, the line of equal magnification is

$$z_m = \frac{\mathrm{e}^{\mathrm{i}\phi}}{m^{1/2}}\left(1+\frac{|\gamma|}{m}\mathrm{e}^{2\mathrm{i}\phi}\right)^{-1/2} = \sum_{k=0}^{\infty}\frac{(-1)^k}{k!}\left(\frac{1}{2}\right)_k\frac{|\gamma|^k}{m^{k+1/2}}\mathrm{e}^{(2k+1)\mathrm{i}\phi}. \tag{68}$$

This is a single simply-connected curve. The areas under it and its derivative are

$$\begin{aligned} S[z_m] &= \sum_{k=0}^{\infty}\frac{2\Gamma(k+3/2)\Gamma(k+1/2)}{\Gamma(k+1)^2}\frac{|\gamma|^{2k}}{m^{2k+1}} \\ &= \frac{\pi}{m}\,{}_2F_1\left(\frac{1}{2},\frac{3}{2};1;\frac{|\gamma|^2}{m^2}\right) \end{aligned} \tag{69}$$

$$\begin{aligned} \frac{\mathrm{d}S[z_m]}{\mathrm{d}m} &= -\sum_{k=0}^{\infty}\frac{4\Gamma(k+3/2)^2}{\Gamma(k+1)^2}\frac{|\gamma|^{2k}}{m^{2k+2}} \\ &= -\frac{\pi}{m^2}\,{}_2F_1\left(\frac{3}{2},\frac{3}{2};1;\frac{|\gamma|^2}{m^2}\right) \end{aligned} \tag{70}$$

The derivative can simply be transported to the source domain by multiplying by the Jacobian determinant (i.e., the inverse magnification), namely

$$\left|\frac{\mathrm{d}S[\zeta_m]}{\mathrm{d}m}\right| = |m^2-1|\left|\frac{\mathrm{d}S[z_m]}{\mathrm{d}m}\right| = \frac{\pi|m^2-1|}{m^2}\,{}_2F_1\left(\frac{3}{2},\frac{3}{2};1;\frac{|\gamma|^2}{m^2}\right). \tag{71}$$

The 'area' under the curve

$$\zeta_m = \sum_{k=0}^{\infty}C_k\left[\frac{(2k-1)\mathrm{e}^{(2k+1)\mathrm{i}\phi}}{2m^{k+1/2}} + \frac{(2k+1)\mathrm{e}^{-(2k-1)\mathrm{i}\phi}}{2m^{k-1/2}}\right]|\gamma|^k \tag{72}$$

(where C_k is given by equation 53), is in principle found either by integrating this or by a similar method as in section 5, the result however is not necessarily the actual area since the curve ζ_m may self-intersect, but the signed sum of the areas of adjacent simply-connected regions.

If $|\gamma| > m \geqslant 0$, we find that the loci of the equally magnified images

$$z_m = \pm\frac{1}{|\gamma|^{1/2}}\left(1+\frac{m}{|\gamma|}\mathrm{e}^{-2\mathrm{i}\phi}\right)^{-1/2} = \pm\sum_{k=0}^{\infty}\frac{(-1)^k}{k!}\left(\frac{1}{2}\right)_k\frac{m^k}{|\gamma|^{k+1/2}}\mathrm{e}^{-2k\mathrm{i}\phi} \tag{73}$$

are two separate mirror-symmetric simply-connected curves. The area and its derivative for one of the simply-connected curves is

$$\begin{aligned} S[z_m] &= \sum_{k=0}^{\infty}\frac{\Gamma(k+3/2)^2}{\Gamma(k+1)\Gamma(k+2)}\frac{m^{2k+2}}{|\gamma|^{2k+3}} \\ &= \frac{\pi m^2}{4|\gamma|^3}\,{}_2F_1\left(\frac{3}{2},\frac{3}{2};2;\frac{m^2}{|\gamma|^2}\right) \end{aligned} \tag{74}$$

$$\begin{aligned} \frac{\mathrm{d}S[z_m]}{\mathrm{d}m} &= \sum_{k=0}^{\infty}\frac{2\Gamma(k+3/2)^2}{\Gamma(k+1)^2}\frac{m^{2k+1}}{|\gamma|^{2k+3}} \\ &= \frac{\pi m}{2|\gamma|^3}\,{}_2F_1\left(\frac{3}{2},\frac{3}{2};1;\frac{m^2}{|\gamma|^2}\right), \end{aligned} \tag{75}$$

whereas

$$\left|\frac{\mathrm{d}S[\zeta_m]}{\mathrm{d}m}\right| = \frac{\pi m|1-m^2|}{2|\gamma|^3}\,{}_2F_1\left(\frac{3}{2},\frac{3}{2};1;\frac{m^2}{|\gamma|^2}\right) \tag{76}$$

where

$$\zeta_m = \mp\sum_{k=0}^{\infty}C_k\frac{km^{k-1}\mathrm{e}^{-2(k-1)\mathrm{i}\phi}+(k-1)m^k\mathrm{e}^{2k\mathrm{i}\phi}}{|\gamma|^{k-1/2}}. \tag{77}$$

Now, if $|\gamma| > 1 > m \geqslant 0$, equation (76) provides us with the distribution of the magnification of all positive parity image(s) for a given source position because there is at most one positive parity image for any source position for $|\gamma| > 1$. More importantly, the total magnification accounting both positive and negative parity images when the source lies within the deltoid caustics is given by

$$M_{\rm tot} = \frac{2}{1-m^2}+\frac{1}{|\gamma|^2-1}\,; \qquad \frac{\mathrm{d}M_{\rm tot}}{\mathrm{d}m} = \frac{4m}{(1-m^2)^2}, \tag{78}$$

and thus,

$$\begin{aligned} P(M_{\rm tot}) &\propto \left|\frac{\mathrm{d}S[\zeta_m]}{\mathrm{d}m}\frac{\mathrm{d}m}{\mathrm{d}M_{\rm tot}}\right| = \frac{\pi|1-m^2|^3}{8|\gamma|^3}\,{}_2F_1\left(\frac{3}{2},\frac{3}{2};1;\frac{m^2}{|\gamma|^2}\right) \\ &= \frac{\pi}{|\gamma|^3}\left(M_{\rm tot}-\frac{1}{|\gamma|^2-1}\right)^{-3}{}_2F_1\left(\frac{3}{2},\frac{3}{2};1;\frac{m^2}{|\gamma|^2}\right) \end{aligned} \tag{79}$$

where

$$m^2 = 1-2\left(M_{\rm tot}-\frac{1}{|\gamma|^2-1}\right)^{-1}. \tag{80}$$

Since $0 \leqslant m < 1$, we have

$$M_{\rm tot} \geqslant M^{\rm c}_{\rm min} = \frac{2|\gamma|^2-1}{|\gamma|^2-1}. \tag{81}$$

While equation (79) is an exact analytic expression for the conditional distribution of the magnification for a source within the deltoid caustics of the Chang–Refsdal lens with $|\gamma| > 1$, the elliptic integrals (to which the hypergeometric function reduces; see Appendix A) are not the most convenient functions to deal with, and therefore, it may be better to come up with a simple and reasonable approximation. First, we note that the leading term of the Taylor-series expansion of equation (79) at $M_{\rm tot} = \infty$ is found to be

$$\left|\frac{\mathrm{d}S[\zeta_m]}{\mathrm{d}M_{\rm tot}}\right| \simeq \frac{\pi}{|\gamma|^3}\,{}_2F_1\left(\frac{3}{2},\frac{3}{2};1;\frac{1}{|\gamma|^2}\right)\cdot M_{\rm tot}^{-3}+\mathscr{O}(M_{\rm tot}^{-4}), \tag{82}$$

which confirms the general result on the asymptotic form of the magnification distribution ($\sim M^{-3}$). Next, we consider the limiting value at $M^{\rm c}_{\rm min} = (2|\gamma|^2-1)/(|\gamma|^2-1)$, that is, $\mathrm{d}S[\zeta_m]/\mathrm{d}M_{\rm tot} = \pi/(2|\gamma|)^3$. We find that the coefficient for the leading term of the Taylor series is approximately equal to $\pi[M^{\rm c}_{\rm min}/(2|\gamma|)]^3$ for $\gamma \gtrsim 1.1$. In other words, the approximation of the distribution by a simple truncated power-law

$$P(M_{\rm tot}) \approx P(M^{\rm c}_{\rm min})\left(\frac{M_{\rm tot}}{M^{\rm c}_{\rm min}}\right)^{-3}\Theta(M_{\rm tot}-M^{\rm c}_{\rm min}) \tag{83}$$

extending down to the minimum magnification (eq. 81) is in fact a reasonably good approximation for $\gamma \gtrsim 1.1$.

Since we have the expression for the full magnification distribution, the mean magnification for the source within the deltoid caustics may be derived from the normalized moment. However, the same special property of having one positive parity image together with the existence of the magnification invariant indicates that it can be derived from the ratio of the areas under the caustics and the critical curve. That is to say, for sources within the deltoid caustics, their corresponding positive parity images completely fill the region inside the critical curve, and thus, the ratio of the area under the critical curve to that under the caustic

$$\langle M_+\rangle = \frac{2\,{}_2F_1(3/2,3/2;2;|\gamma|^{-2})}{{}_2F_1(3/2,3/2;3;|\gamma|^{-2})} \tag{84}$$

gives the mean magnification of the positive parity image. Finally, equation (20) implies that the mean total magnification $\langle M_{\rm tot}\rangle$ for this case is related to the mean magnification of the positive parity image $\langle M_+\rangle$ through

$$\langle M_{\rm tot}\rangle = 2\langle M_+\rangle+\frac{1}{|\gamma|^2-1} = \frac{4|\gamma|^2}{|\gamma|^2-1}\frac{{}_2F_1(1/2,3/2;2;|\gamma|^{-2})}{{}_2F_1(3/2,3/2;3;|\gamma|^{-2})}. \tag{85}$$

Using this result, we can also derive the analytic expression for the area under the pre-caustics in equation (65) as

$$S[z_{\rm p}] = \langle M_{\rm tot}\rangle S[\zeta_{\rm c}] = \frac{\pi}{2|\gamma|(|\gamma|^2-1)}\,{}_2F_1\left(\frac{1}{2},\frac{3}{2};2;\frac{1}{|\gamma|^2}\right). \tag{86}$$

7 A CONVERGENT BACKGROUND

One possible generalization of the Chang–Refsdal lens equation (2) is the addition of a constant convergence term

$$\zeta = z-\frac{1}{\bar{z}}-\gamma\bar{z}-\kappa z, \tag{87}$$

which describes a continuous mass distribution with a constant surface density. While the effect of the constant convergence term (κz) is basically an overall magnification (uniform defocusing) of the lens domain with respect to the source domain, the specific behaviour of the lensed images is quite distinct, depending on the sign of $(1-\kappa)$. If $0 \leqslant \kappa < 1$ (note that κ must be non-negative and real since Poisson's equation indicates that κ is simply the rescaled surface mass density), introductions of new variables $\eta = \zeta/(1-\kappa)^{1/2}$, $\xi = (1-\kappa)^{1/2}z$, and $g = \gamma/(1-\kappa)$ simply reduce the lens equation to the form of equation (2) (Paczyński 1986). Hence, the lensing behaviour of these systems basically follows that of the standard Chang–Refsdal lens discussed so far, except for the use of the 'reduced shear' $g = \gamma/(1-\kappa)$ and the additional focusing factor $(1-\kappa)$ in the magnification.

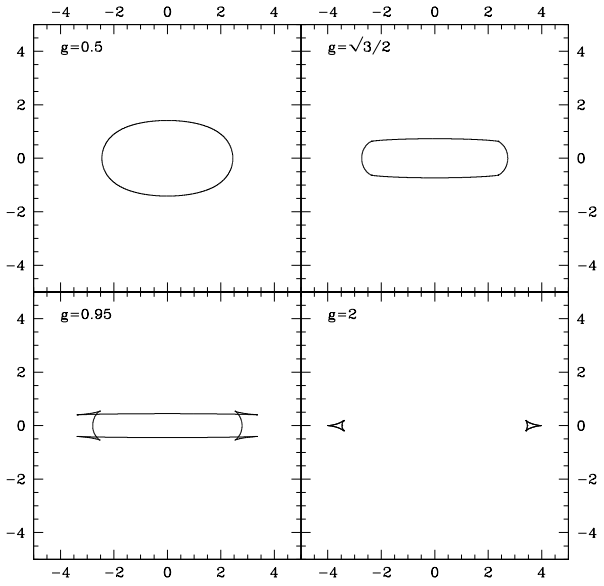

Figure 6. Caustics for the Chang–Refsdal lens with additional background convergence in the cases $g = 1/2$, $\sqrt{3}/2$, 0.95, and 2.

However, for $\kappa > 1$, which is sometimes referred to as the over-focusing case, the introduction of the rescaled variables leaves the sign of the point-mass deflection term changed. With $\eta = -\zeta/(\kappa-1)^{1/2}$, $\xi = (\kappa-1)^{1/2}z$, and $g = \gamma/(\kappa-1)$, we have the lens equation

$$\eta = \xi + \frac{1}{\bar{\xi}} + g\bar{\xi}. \tag{88}$$

At the limit of $g = 0$, the system allows two images

$$\xi = \frac{\eta}{2}\left[1 \pm \left(1 - \frac{4}{|\eta|^2}\right)^{1/2}\right] \tag{89}$$

if $|\eta| \geqslant 2$, whereas no image is formed if $|\eta| < 2$. The total magnification for $|\eta| \geqslant 2$ is given by

$$(1-\kappa)^2 M_{\rm tot} = \frac{|\eta|^2 - 2}{|\eta|\sqrt{|\eta|^2 - 4}} \tag{90}$$

where the $(1-\kappa)^2$ factor is due to the overall focusing factor. Note that the magnification diverges at $|\eta| = 2$ indicating that the caustic of this system is given by the circle $|\eta| = 2$. The corresponding critical curve is found to be another circle $|\xi| = 1$. For this system, when the source crosses the caustic into its interior, two images, one inside and the other outside of the critical curve divergently merge and vanish. Two images re-appear when the source crosses the caustics outwards.

For the general case when $g \neq 0$, the lensing behaviour can be studied using the same methods developed throughout this paper. For example, the image positions can be found by solving similar rational equations or polynomials as equations (6) and (7), but with the following replacement of variables: $z \to \xi$, $\gamma \to g$, $\bar{\gamma} \to \bar{g}$, $\zeta \to \eta$, and $\bar{\zeta} \to -\bar{\eta}$. One notable difference between the new polynomial equation as compared to that of the standard Chang–Refsdal lens is that it has a quadruple zero if $g = \sqrt{3}/2$ and $2\eta = \pm(3+\sqrt{3}) \pm (3-\sqrt{3})$i, which indicates that this system will exhibit third-order critical behaviour, namely the swallow-tail catastrophe along the caustics, for $g = \sqrt{3}/2$. In fact, this result can be more easily obtained by analysis of the lens mapping along the lines of section 5.

In Fig. 6, we plot the caustics for these systems with $g = 1/2$, $\sqrt{3}/2$, 0.95, and 2. The topology of the critical curves are basically the same as the standard null-convergent Chang–Refsdal lens. If $0 \leqslant g < \sqrt{3}/2$, the caustics are the oval-shape cuspless curve, within which no image is formed. At $g = \sqrt{3}/2$, the caustic becomes a pin-cushion shape with a swallow-tail catastrophe at its four corners. Again, the system allows two image outside the caustics and no image inside the caustic. For $\sqrt{3}/2 < g < 1$, the swallow-tail catastrophe of the caustics metamorphoses to self-intersecting curves with two cusps at each of four corners. There exist four images for the source within the fish-tail-like region of the caustics, while there is still no image for the source within the main pillow-like region of the caustics. As for $g > 1$, there appear two deltoid-like caustics, but unlike the standard null-convergent case, the caustics are stretched in the length direction rather than the width direction.

While a more detailed study of the lensing behaviour can be easily done, it is beyond our scope here. However, we note that such a study may help understand the distinct microlensing behaviour of the central demagnified macro-image at the maximum of the time-delay surface (see e.g. Dobler, Keeton, & Wambsganss 2005).

8 *N* POINT MASSES WITH SHEAR

Another physically interesting generalization of the Chang–Refsdal lens is to the case of N point masses with shear. This can be represented by the lens equation

$$\zeta = z - \sum_i \frac{m_i}{\bar{z} - \bar{l}_i} - \gamma\bar{z}, \tag{91}$$

where m_i are the relative masses and l_i are the complex positions. We find that the deflection function (c.f., eq. 3)

$$s(z) = \sum_i^N \frac{m_i}{z - l_i} + \bar{\gamma}z = \frac{\bar{\gamma}z\prod_i^N (z-l_i) + \sum_i^N m_i \prod_{j\neq i}^N (z-l_j)}{\prod_i^N (z-l_i)} \tag{92}$$

is a rational function of degree $(N+1)$, where N is the number of point masses. To establish the imaging equation, we follow the same procedure as in section 3. This leads to consideration of the rational equation $g(z) = z - h(z)$, or equivalently the fixed points of the mapping $h(z) = (\bar{f}\circ f)(z)$ where $f(z) = \bar{\zeta} + s(z)$ and $\bar{f}(w) = \overline{f(\bar{w})}$. Here, since $f(z)$ is of degree $(N+1)$, $h(z)$ is of degree $(N+1)^2$. In addition, as $z \to \infty$, $s(z)$ [and consequently $f(z)$] diverges linearly ($\gamma \neq 0$) and so does $h(z)$. This indicates that the degree of the rational function $g(z)$, as well as the order of the polynomial in its numerator, is $(N+1)^2$ (Witt 1990). Obviously, as N grows, finding image positions through solving $(N+1)^2$-th order polynomial equation quickly becomes impractical. On the other hand, the parametric representation of the critical curves (and subsequently the caustics) can be derived from $|s'(z)|^2 = 1$ or by simply solving $s'(z) = -e^{-2i\phi}$, which reduces to a $(2N)$-th order polynomial equation. Here, the parameter ϕ is chosen such that ϕ is the argument angle of the tangent to the caustics (section 5). In other words, finding the critical curves and the caustics is comparatively easier as the order of the relevant polynomial grows linearly with N. By contrast, solving the lens equation requires us to solve a polynomial whose order grows quadratically as N increases.

One additional point to note regarding the N point mass lenses under constant external shear is that, despite the order of the imaging polynomial being $(N+1)^2$, the upper bound for the number of images grows linearly with N. Using the result of Appendix

B, we find that the total number of images for a lens system with N point masses with non-zero shear may not be greater than $5(N + 1) - 6 = 5N - 1$. [Compare this to the upper bound for $\gamma = 0$, which is $5(N - 1)$ with $N \geqslant 2$ (Rhie 2001, 2003) and for which the order of the corresponding imaging polynomial is $N^2 + 1$ (Witt 1990).] This also means that the imaging polynomial must have a zero that is not a image position if $N \geqslant 3$ (for $\gamma \neq 0$ and $|\gamma| \neq 1$). Furthermore, if $0 < |\gamma| < 1$, we find that $n_+ \leqslant 2N$ and $n_- - n_+ = N - 1$ where n_+ and n_- are the numbers of positive and negative parity images, respectively. For $|\gamma| > 1$, these results become $n_+ \leqslant 2N - 1$ and $n_- - n_+ = N + 1$.

We note that, for the least extreme case (i.e., the source 'outside' the caustics), the difference in the number of opposite parity images can be understood as being due to one negative parity image associated with each point mass, plus one additional image of either positive ($0 < |\gamma| < 1$) or negative ($|\gamma| > 1$) parity. Here, the one additional image of 'spare' parity can be regarded as the weakly perturbed macro image: the system with $0 < |\gamma| < 1$ represents the macro image at the 'minimum' in the time-delay surface (the positive parity image at sub-unity convergence), while that with $|\gamma| > 1$ corresponds to the macro image at the 'saddle point' in the time-delay surface (the negative parity image).

9 CONCLUSIONS

This paper has presented a complete mathematical treatment of the Chang–Refsdal lens. This simple and flexible model has found widespread applications in astrophysics. The lens equation for the Chang–Refsdal lens can be converted to a polynomial of the fourth degree, the roots of which provide the image locations (together with possibly spurious roots). If the source lies on one of the symmetry axes with respect to the external shear, this quartic readily factorizes into a product of quadratics, which enables the lens equation to be solved via elementary means for these special cases. Simple lensing invariants exist for the products of the (complex) positions of the four images, as well as for sums of the moments of their signed magnifications. In other words, provided the source lies within the astroid or deltoid caustics, the sums of signed magnification, multiplied by moments of the complex positions, are invariant.

Of the results in this paper, we highlight just two here. First, we have provided the equations for the pre-caustics. Only one other lens model has been known for which the pre-caustics can be written down, namely the singular isothermal sphere with external shear (Finch et al. 2002). Second, the exact analytical expression (eq. 79) in terms of hypergeometric functions (or elliptic integrals) has been calculated for the distribution of magnifications for the source within the deltoid caustics of the Chang–Refsdal lens. For many practical purposes, however, we have shown that a truncated power-law (eq. 83) is an excellent approximation to this distribution. There are a number of applications of these two results. For example, the Chang–Refsdal lens is often used as an approximation to the binary lens equation, especially in the case when the lens is a star plus planet. The areas under the critical curves and pre-caustics are directly related to the mean magnifications of the 2 and 4 image geometries. and hence the detectability of a planet through the gravitational microlensing effect. Equally, the distribution of magnifications is applicable to the statistics of high-magnification microlensing events in the lightcurves of quasars.

ACKNOWLEDGMENTS

The authors thank Olaf Wucknitz for a number of helpful comments. JA acknowledges A. O. Petters for pointing the result of Khavinson & Neumann (2006), and P. L. Schechter for that of Finch et al. (2002). Work by JA at Cambridge (UK) was supported though the grants from the Leverhume Trust Foundation and the Particle Physics and Astronomy Research Council (UK). JA at MIT is supported through the grants AST-0433809 and AST-0434277 from the National Science Foundation (US). Gravitational lensing at Cambridge (UK) is supported by the Astrophysics Network for Galaxy LEnsing Studies (ANGLES), funded by the European Union.

REFERENCES

Abramowitz M., Stegun I. A., 1972, Handbook of Mathematical Functions. Dover, New York
Alexander T., Loeb A., 2001, ApJ, 551, 223 (astro-ph/0009404)
An J. H., 2005, MNRAS, 356, 1409 (astro-ph/0410388)
Asada H., 2002, A&A, 390, L11 (astro-ph/0206267)
Asada H., Kasai T., Kasai M., 2004, Progress Theor. Phys., 112, 241 (astro-ph/0407597)
Berndt B. C., 1985, Ramanujan's Notebooks, Part I. Springer-Verlag, Berlin
Bourassa R. R., Kantowski R., 1975, ApJ, 195, 13
Bozza V., 1999, A&A, 348, 311 (astro-ph/9904297)
Bozza V., 2000, A&A, 355, 423 (astro-ph/9910535)
Burke W. L., 1981, ApJ, 244, L1
Carleson L., Gemelin T. W., 1993, Complex Dynamics. Springer-Verlag, Berlin
Carlson B. C., 1977, SIAM J. Math. Analysis, 8, 231
Chang K., Refsdal S., 1979, Nature, 282, 561
Chang K., Refsdal S., 1984, A&A, 132, 168
Dalal N., Rabin J. M., 2001, J. Math. Phys., 42, 4 (astro-ph/0009002)
Dobler G., Keeton C. R., Wambsganss J., 2005, MNRAS, submitted (astro-ph/0507522)
Dominik M., 1998, A&A, 333, L79 (astro-ph/9804059)
Dominik M., 1999, A&A, 349, 108 (astro-ph/9903014)
Erdélyi, A., Magnus W., Oberhettinger F., Tricomi F. G., 2006 Higher Transcendental Functions. Dover, New York
Evans N. W., Hunter C., 2002, ApJ, 575, 68 (astro-ph/0204206)
Finch T. K., Carlivati L. P., Winn J. N., Schechter P. L., 2002, ApJ, 577, 51 (astro-ph/0205489)
Gaudi B. S., Gould A., 1997, ApJ, 486, 85 (astro-ph/9610123)
Gould A., Gaucherel C., 1997, ApJ, 477, 580 (astro-ph/9606105)
Gould A., Loeb A., 1992, ApJ, 396, 104
Gradshteyn I. S., Ryzhik I. M., 2000, Tables of Integrals, Series, and Products, 6th edn. Academic Press, London
Hunter C., Evans N. W., 2001, ApJ, 554, 1227 (astro-ph/0102081)
Khavinson D., Neumann G., 2006, Proc. Am. Math. Soc., 134, 1077 (math.CV/0401188)
Khavinson D., Świątek G., 2003, Proc. Am. Math. Soc., 131, 409
Kovner I., 1987, ApJ, 312, 22
Paczyński B., 1986, ApJ, 301, 503
Petters A., Levine J., Wambsganss J., 2001, Singularity Theory and Gravitational Lensing. Birkhäuser, Boston
Press W. H., Teukolsky S. A., Vetterling W. T., Flannery B. P., 1992, Numerical Recipes in FORTRAN 77, 2nd edn. Cambridge Univ. Press, Cambridge
Rhie S. H., 2001, arXiv Astrophys. preprint, arXiv:astro-ph/0103463
Rhie S. H., 2002, arXiv Astrophys. preprint, arXiv:astro-ph/0207612
Rhie S. H., 2003, arXiv Astrophys. preprint, arXiv:astro-ph/0305166
Schneider P., 1987, ApJ, 319, 9
Schneider P., Ehlers J., Falco E. E., 1992, Gravitational Lenses. Springer-Verlag, Berlin
Schramm T., Kayser R., 1995, A&A, 299, 1 (astro-ph/9408064)
Subramanian K., Chitre S. M., Narasimha D., 1985, ApJ, 289, 37
Witt H. J., 1990, A&A, 236, 311
Witt H. J., Mao S., 1995, ApJ, 447, L105
Witt H. J., Mao S., 2000, MNRAS, 311, 689 (astro-ph/9906323)

APPENDIX A: ELLIPTIC INTEGRALS FROM HYPERGEOMETRIC FUNCTIONS

We note that all hypergeometric functions found in the main text reduce to expressions involving elliptic integrals. Although the generality of the hypergeometric function can be seen as grounds for superiority, there are some advantages in using elliptic integrals especially for computational purpose, partly because numerical routines to evaluate elliptic integrals are more readily available than hypergeometric functions (see e.g. Press et al. 1992). For this reason, and also to help readers compare results to those found in the

literature, we provide alternative expressions written in terms of elliptic integrals.

First, we note a relationship between hypergeometric functions with parameters differing by unity;

$$ {}_2F_1\,(a,b;c;x) - {}_2F_1\,(a-1,b;c;x) = \frac{b}{c}x\,{}_2F_1\,(a,b+1;c+1;x)\,, $$

and one of the Euler transformations of the hypergeometric functions;

$$ {}_2F_1\,(a,b;c;x) = (1-x)^{c-a-b}\,{}_2F_1\,(c-a,c-b;c;x)\,. $$

Using these two, we can express any Gaussian hypergeometric function ${}_2F_1(a,b;c;x)$ with a and b being half-integers and c a positive integer in terms of a linear combination of ${}_2F_1(1/2,1/2;1;x)$ and ${}_2F_1(-1/2,1/2;1;x)$ with the coefficients being rational functions of x. However, the complete elliptic integrals of the first and the second kind are actually hypergeometric functions

$$ \begin{aligned} \mathbf{K}(k) &\equiv \int_0^{\pi/2} \frac{\mathrm{d}\phi}{\sqrt{1-k^2\sin^2\phi}} = \frac{\pi}{2}\,{}_2F_1\left(\frac{1}{2},\frac{1}{2};1;k^2\right) \\ \mathbf{E}(k) &\equiv \int_0^{\pi/2} \mathrm{d}\phi\,\sqrt{1-k^2\sin^2\phi} = \frac{\pi}{2}\,{}_2F_1\left(-\frac{1}{2},\frac{1}{2};1;k^2\right). \end{aligned} $$

In other words, the hypergeometric function ${}_2F_1(a,b;c;k^2)$ is in general expressible in terms of the complete elliptic integrals if a and b are half-integers and c is a positive integer. For example,

$$ \begin{aligned} \frac{\pi}{2}\,{}_2F_1\left(\frac{1}{2},\frac{3}{2};1;k^2\right) &= \frac{\mathbf{E}(k)}{1-k^2} \\ \frac{\pi}{2}\,{}_2F_1\left(-\frac{1}{2},\frac{3}{2};1;k^2\right) &= 2\mathbf{E}(k) - \mathbf{K}(k) \\ \frac{\pi}{2}\,{}_2F_1\left(-\frac{1}{2},-\frac{1}{2};1;k^2\right) &= 2\mathbf{E}(k) - (1-k^2)\mathbf{K}(k) \end{aligned} $$

etc. Further examples can be found in standard references such as Erdélyi et al. (2006), Abramowitz & Stegun (1972), or Gradshteyn & Ryzhik (1994), or on-line resources like Wolfram Research site[4]. (Be careful as many authors use various different conventions for the arguments of the elliptic integrals!)

From these, we find alternative expressions written in terms of elliptic integrals for equations (54) and (55);

$$ S\,[z_\mathrm{c}] = \frac{2\mathbf{E}\,(|\gamma|)}{1-|\gamma|^2} \tag{A1} $$

$$ S\,[\zeta_\mathrm{c}] = 2\pi + 4\mathbf{K}\,(|\gamma|) - 8\mathbf{E}\,(|\gamma|)\,, \tag{A2} $$

for equations (59) and (60);

$$ S\,[z_\mathrm{c}] = \frac{|\gamma|}{|\gamma|^2-1}\mathbf{E}\left(\frac{1}{|\gamma|}\right) - \frac{1}{|\gamma|}\mathbf{K}\left(\frac{1}{|\gamma|}\right) \tag{A3} $$

$$ S\,[\zeta_\mathrm{c}] = \frac{2(2|\gamma|^2-1)}{|\gamma|}\mathbf{K}\left(\frac{1}{|\gamma|}\right) - 4|\gamma|\mathbf{E}\left(\frac{1}{|\gamma|}\right), \tag{A4} $$

for equations (69), (70), and (71);

$$ S\,[z_m] = \frac{2m}{m^2-|\gamma|^2}\mathbf{E}\left(\frac{|\gamma|}{m}\right) \tag{A5} $$

$$ \frac{\mathrm{d}S\,[z_m]}{\mathrm{d}m} = \frac{2}{m^2-|\gamma|^2}\left[\mathbf{K}\left(\frac{|\gamma|}{m}\right) - \frac{2m^2}{m^2-|\gamma|^2}\mathbf{E}\left(\frac{|\gamma|}{m}\right)\right] \tag{A6} $$

$$ \left|\frac{\mathrm{d}S\,[\zeta_m]}{\mathrm{d}m}\right| = \frac{2|m^2-1|}{m^2-|\gamma|^2}\left[\frac{2m^2}{m^2-|\gamma|^2}\mathbf{E}\left(\frac{|\gamma|}{m}\right) - \mathbf{K}\left(\frac{|\gamma|}{m}\right)\right], \tag{A7} $$

for equations (74), (75), and (76);

$$ S\,[z_m] = \frac{|\gamma|}{|\gamma|^2-m^2}\mathbf{E}\left(\frac{m}{|\gamma|}\right) - \frac{1}{|\gamma|}\mathbf{K}\left(\frac{m}{|\gamma|}\right) \tag{A8} $$

$$ \frac{\mathrm{d}S\,[z_m]}{\mathrm{d}m} = \frac{m}{|\gamma|(|\gamma|^2-m^2)}\left[\frac{2|\gamma|^2}{|\gamma|^2-m^2}\mathbf{E}\left(\frac{m}{|\gamma|}\right) - \mathbf{K}\left(\frac{m}{|\gamma|}\right)\right] \tag{A9} $$

$$ \left|\frac{\mathrm{d}S\,[\zeta_m]}{\mathrm{d}m}\right| = \frac{m|1-m^2|}{|\gamma|(|\gamma|^2-m^2)}\left[\frac{2|\gamma|^2}{|\gamma|^2-m^2}\mathbf{E}\left(\frac{m}{|\gamma|}\right) - \mathbf{K}\left(\frac{m}{|\gamma|}\right)\right], \tag{A10} $$

and for equation (86);

$$ S\,[z_\mathrm{p}] = \frac{2|\gamma|}{|\gamma|^2-1}\left[\mathbf{K}\left(\frac{1}{|\gamma|}\right) - \mathbf{E}\left(\frac{1}{|\gamma|}\right)\right]. \tag{A11} $$

In the literature, sometimes results are given in terms of the incomplete elliptic integrals even if they are entirely expressible using only the complete elliptic integrals. Let us consider the Jacobi form of the incomplete elliptic integrals of the first and the second kind;

$$ \begin{aligned} \mathrm{F}(s;k) &\equiv \int_0^s \frac{\mathrm{d}v}{(1-v^2)^{1/2}(1-k^2v^2)^{1/2}} \\ \mathrm{E}(s;k) &\equiv \int_0^s \frac{(1-k^2v^2)^{1/2}}{(1-v^2)^{1/2}}\,\mathrm{d}v. \end{aligned} $$

Here, we note that $\mathbf{K}(k) = \mathrm{F}(1;k)$ and $\mathbf{E}(k) = \mathrm{E}(1;k)$. Then, we find that, with $s = 1/k = z^{-1}$,

$$ \begin{aligned} \mathrm{F}\left(\frac{1}{z};z\right) &= \int_0^{1/z} \frac{\mathrm{d}v}{(1-v^2)^{1/2}(1-z^2v^2)^{1/2}} \\ &= \int_0^1 \frac{\mathrm{d}w/z}{(1-w^2/z^2)^{1/2}(1-w^2)^{1/2}} = \frac{1}{z}\,\mathbf{K}\left(\frac{1}{z}\right) \\ \mathrm{E}\left(\frac{1}{z};z\right) &= \int_0^{1/z} \frac{(1-z^2v^2)^{1/2}}{(1-v^2)^{1/2}}\,\mathrm{d}v = \int_0^1 \frac{(1-w^2)^{1/2}}{(1-w^2/z^2)^{1/2}}\,\frac{\mathrm{d}w}{z} \\ &= \int_0^1 \frac{1-z^2+z^2(1-w^2/z^2)}{(1-w^2)^{1/2}(1-w^2/z^2)^{1/2}}\,\frac{\mathrm{d}w}{z} \\ &= \frac{1-z^2}{z}\mathbf{K}\left(\frac{1}{z}\right) + z\,\mathbf{E}\left(\frac{1}{z}\right) \end{aligned} $$

so that $z^{-1}\mathbf{K}(z^{-1}) = \mathrm{F}(z^{-1};z)$ and $z\mathbf{E}(z^{-1}) = \mathrm{E}(z^{-1};z) - (1-z^2)\mathrm{F}(z^{-1};z)$. From this, we also find expressions using incomplete elliptic integrals for equations (A3) and (A4);

$$ S\,[z_\mathrm{c}] = \frac{1}{|\gamma|^2-1}\mathrm{E}\left(\frac{1}{|\gamma|};|\gamma|\right) \tag{A12} $$

$$ S\,[\zeta_\mathrm{c}] = 2\mathrm{F}\left(\frac{1}{|\gamma|};|\gamma|\right) - 4\mathrm{E}\left(\frac{1}{|\gamma|};|\gamma|\right), \tag{A13} $$

for equations (A8) and (A9);

$$ S\,[z_m] = \frac{m}{|\gamma|^2-m^2}\mathrm{E}\left(\frac{m}{|\gamma|};\frac{|\gamma|}{m}\right) \tag{A14} $$

$$ \frac{\mathrm{d}S\,[z_m]}{\mathrm{d}m} = \frac{1}{|\gamma|^2-m^2}\left[\frac{2m^2}{|\gamma|^2-m^2}\mathrm{E}\left(\frac{m}{|\gamma|};\frac{|\gamma|}{m}\right) + \mathrm{F}\left(\frac{m}{|\gamma|};\frac{|\gamma|}{m}\right)\right], \tag{A15} $$

and for equation (A11)

$$ S\,[z_\mathrm{p}] = \frac{2}{|\gamma|^2-1}\left[\mathrm{F}\left(\frac{1}{|\gamma|};|\gamma|\right) - \mathrm{E}\left(\frac{1}{|\gamma|};|\gamma|\right)\right]. \tag{A16} $$

Press et al. (1992) incorporated the so-called Carlson (1977) symmetric form of the elliptic integrals, which may be advantageous for certain considerations over the conventional Legendre-Jacobi standard form. Two of Carlson's integrals are used to re-

[4] `http://functions.wolfram.com`

express the elliptic integrals of the first and the second kinds:

$$R_F(x,y,z) \equiv \frac{1}{2}\int_0^\infty (t+x)^{-1/2}(t+y)^{-1/2}(t+z)^{-1/2}\,dt$$
$$R_D(x,y,z) \equiv \frac{3}{2}\int_0^\infty (t+x)^{-1/2}(t+y)^{-1/2}(t+z)^{-3/2}\,dt.$$

From the Jacobi form of the integrals given above, by changing the integration variable to $t = (s/v)^2 - 1$, it is easy to establish the transformations:

$$\mathrm{F}(s;k) = sR_F(1-s^2, 1-k^2s^2, 1)$$
$$\mathrm{E}(s;k) = sR_F(1-s^2, 1-k^2s^2, 1) - \frac{k^2s^3}{3}R_D(1-s^2, 1-k^2s^2, 1),$$

and subsequently, $\mathbf{K}(k) = R_F(0, 1-k^2, 1)$ and $\mathbf{E}(k) = R_F(0, 1-k^2, 1) - (k^2/3)R_D(0, 1-k^2, 1)$. Using this, we can re-express equations (A1) and (A2)

$$S[z_c] = \frac{2}{1-|\gamma|^2}\left[R_F\left(0, c^2, 1\right) - \frac{|\gamma|^2}{3}R_D\left(0, c^2, 1\right)\right]$$
$$S[\zeta_c] = 2\pi + \frac{8}{3}|\gamma|^2 R_D\left(0, c^2, 1\right) - 4R_F\left(0, c^2, 1\right)$$

where $c^2 = 1 - |\gamma|^2$, equations (A3) and (A4)

$$S[z_c] = \frac{1}{|\gamma|(|\gamma|^2-1)}\left[R_F\left(0, q^2, 1\right) - \frac{1}{3}R_D\left(0, q^2, 1\right)\right]$$
$$S[\zeta_c] = \frac{1}{|\gamma|}\left[\frac{4}{3}R_D\left(0, q^2, 1\right) - 2R_F\left(0, q^2, 1\right)\right]$$

where $q^2 = 1 - |\gamma|^{-2}$, equations (A5) and (A6)

$$S[z_m] = \frac{2m}{m^2-|\gamma|^2}\left[R_F\left(0, c_m^2, 1\right) - \frac{|\gamma|^2}{3m^2}R_D\left(0, c_m^2, 1\right)\right]$$
$$\frac{\mathrm{d}S[z_m]}{\mathrm{d}m} = \frac{2}{(m^2-|\gamma|^2)^2}\left[\frac{2}{3}|\gamma|^2 R_D\left(0, c_m^2, 1\right) - (m^2+|\gamma|^2)R_F\left(0, c_m^2, 1\right)\right]$$

where $c_m^2 = 1 - (|\gamma|/m)^2$, equations (A8) and (A9)

$$S[z_m] = \frac{m^2}{|\gamma|(|\gamma|^2-m^2)}\left[R_F\left(0, q_m^2, 1\right) - \frac{1}{3}R_D\left(0, q_m^2, 1\right)\right]$$
$$\frac{\mathrm{d}S[z_m]}{\mathrm{d}m} = \frac{m}{|\gamma|(|\gamma|^2-m^2)^2}\left[(|\gamma|^2+m^2)R_F\left(0, q_m^2, 1\right) - \frac{2}{3}m^2 R_D\left(0, q_m^2, 1\right)\right]$$

where $q_m^2 = 1 - (m/|\gamma|)^2$, and equation (A11)

$$S[z_p] = \frac{2}{3|\gamma|(|\gamma|^2-1)}R_D\left(0, q^2, 1\right).$$

APPENDIX B: THE NUMBER OF IMAGES OF A RATIONAL LENS MAPPING

In this Appendix, we examine the problem: what is the maximum number of images for N point masses with shear? In fact, it is scarcely any more work to consider the more general case of the deflection function that is a rational function of complex position. This problem was in fact solved by Khavinson & Neumann (2006) under still more general considerations. In particular, for the case of N point masses in the absence of shear, their result provides us with an affirmative answer to the conjecture by Rhie (2001, see also Rhie 2003): the maximum number of images for N point masses ($N \geqslant 2$) with no shear is $5(N-1)$. However, while the result of Khavinson & Neumann (2006) is strictly true, the limit can be further lowered depending on the particular behaviour of the rational function, as seen by Khavinson & Świątek (2003). Here, we revisit the proofs of Khavinson & Świątek (2003) and Khavinson & Neumann (2006), and derive specific limits depending on the asymptotic behaviour of the rational lens mapping.

Let us suppose that the lens equation is written as

$$\zeta = z - \overline{s(z)}$$

where $s(z)$ is a rational function of degree $r \geqslant 2$ – i.e, a rational function that is neither a constant function nor a Möbius transformation.[5] Therefore, $s(z) : \mathbb{C}_\infty \to \mathbb{C}_\infty$ is surjective – 'onto' – but not injective – 'one-to-one'. Here $\mathbb{C}_\infty \equiv \mathbb{C} \cup \{\infty\}$ is the 'Riemann sphere.' By considering the complex conjugate, the lens mapping can also be written, after rearranging terms, as

$$\overline{z} = f(z) = \overline{\zeta} + s(z)$$

where $f(z)$ is also a rational function of degree r, and in addition $f'(z) = s'(z)$. Then, the image positions are found among the fixed points of a degree-r^2 rational function $h(z) = (\overline{f} \circ f)(z) = \overline{f}[f(z)]$ or equivalently the zeros of a rational function $g(z) = z - h(z)$. Here, $\overline{f}(w) = \overline{f(\overline{w})}$ is also a degree-r rational function of its argument so that $h(z)$ is in fact a degree-r^2 rational function of z. On the other hand, the degree of $g(z)$ is either r^2+1 if $\lim_{z\to\infty} h(z)$ is finite or r^2 if it is infinite. Actually, if $\lim_{z\to\infty} s(z) = \infty$, then $h(z)$ diverges as $z \to \infty$, whereas $\lim_{z\to\infty} h(z)$ is finite if $\lim_{z\to\infty} s(z) = a$ is finite except for the case when $s(z)$ has a pole at $z = \zeta + \overline{a}$. Here, the incident of the exceptional case explicitly depends on the specific choice of the source position (ζ), and so this cannot be a generic occurrence for any lens system with an arbitrary source location. Hence, ignoring the exceptional cases, we find that the degree of $g(z)$ is either r^2 if $s(z)$ diverges as $z \to \infty$ or r^2+1 if otherwise.

Now, according to the theorem due to Pierre J. L. Fatou (1878-1929) and Gaston M. Julia (1893-1978), we have

Theorem B.1. (Fatou-Julia) *"Every attracting cycle for a rational function (degree $r \geqslant 2$) attracts at least one critical point,"* or equivalently *"Every basin of attraction for a rational map (degree $r \geqslant 2$) contains at least one critical point."*

The proof requires some familiarity with complex analysis, in particular, Schwarz's Lemma and/or the Riemann Mapping Theorem, which is beyond our scope (see e.g. Carleson & Gamelin 1993). Instead, here we simply accept the implications of Theorem B.1 for the current problem as a fact without detailing any proof: For any attracting[6] fixed point of $h(z)$, there is at least one critical point[7] ('stationary point' or 'ramification point') of $h(z)$ that converges to the fixed point under the iterative mapping of $h(z)$, that is to say,

Theorem B.2. *For any point $z_f \in \mathbb{C}_\infty$ that satisfies $h(z_f) = z_f$ and $|h'(z_f)| < 1$, there is at least one point $z_c \in \mathbb{C}_\infty$ such that $h'(z_c) = 0$ and $\lim_{n\to\infty} h^n(z_c) = z_f$.*

Here, $h^2(z) = (h \circ h)(z)$, $h^3(z) = (h \circ h^2)(z)$, and so on. We need to take particular care in the interpretation of $h'(z)$ when $z = \infty$ or $h(z) = \infty$. By considering its composition with the map z^{-1}, we deduce the following:

[5] Formally, this indicates that the image $s(\mathbb{C}_\infty)$ of the Riemann sphere under the given (meromorphic) function $s(z) : \mathbb{C}_\infty \to \mathbb{C}_\infty$ is an r-fold covering of $\mathbb{C}_\infty$. That is, the number of solutions in $\mathbb{C}_\infty$ of $s(z) = a$ (counting multiplicities) is r for any $a \in \mathbb{C}$. With a rational function $s(z) = \mathrm{s_n}(z)/\mathrm{s_d}(z)$ where $\mathrm{s_n}(z)$ and $\mathrm{s_d}(z)$ are polynomials with no common factor, this is basically $r = \max\{\deg \mathrm{s_n}(z), \deg \mathrm{s_d}(z)\}$ where $\deg p(z)$ is the degree or the order of the polynomial $p(z)$.

[6] The fixed point of $h(z)$ is said to be super-attracting, attracting, neutral, or repelling, if $h'(z) = 0$, $|h'(z)| < 1$, $|h'(z)| = 1$, or $|h'(z)| > 1$, respectively.

[7] The critical point of a function is the point at which the mapping given by the function is locally stationary. To avoid any confusion with the critical points of the lens mapping, we will avoid the use of this term in favor of the stationary point. For an analytic function $s(z)$, they are equivalent to zeros of $s'(z)$. However, for a meromorphic function $s(z)$ of Riemann sphere onto itself, this identification should be applied with a caveat due to the association of $\infty^{-1} = 0$. That is, the point at which $s'(z) = \infty^{-n}$ with n is a positive integer is not necessarily a critical point. For example, the mapping $s(z) = z^{-1}$ is regular at $z = \infty$ although $s'(z) = -z^{-2}$. In fact, for the discussion in this appendix, the critical point may be better understood as being a ramification point in the topological sense.

(i) If $h(\infty) = \lim_{z\to\infty} h(z) = \infty$, then $h'(\infty) = \lim_{z\to\infty} z^2 h'(z)/[h(z)]^2$. Specifically, if $h(z) \sim az$ as $z \to \infty$ with $a \neq 0$ being a constant, then $h(\infty) = \infty$ and $|h'(\infty)| = |a|^{-1}$, and if $h(z) \sim az^n$ ($n \geqslant 2$) as $z \to \infty$, then $h(\infty) = \infty$ and $h'(\infty) = 0$.

(ii) If $|h(\infty)| = |\lim_{z\to\infty} h(z)| < \infty$ is finite, then $h'(\infty) = 0$ if and only if $\lim_{z\to\infty} z^2 h'(z) = 0$.

(iii) If $h(z_\mathrm{p}) = \infty$ for a finite z_p, then $h'(z_\mathrm{p}) = 0$ if and only if $\lim_{z\to z_\mathrm{p}} h'(z)/[h(z)]^2 = 0$. In other words, if z_p is a higher-order pole of $h(z)$ than a simple pole, then $h'(z_\mathrm{p}) = 0$.

In the following, we want to prove that Theorem B.2 implies that

Theorem B.3. *For any point $z_0 \in \mathbb{C}_\infty$ that satisfies $f(z_0) = \bar{z}_0$ and $|s'(z_0)| < 1$, there is at least one point $z_\mathrm{c} \in \mathbb{C}_\infty$ such that $s'(z_\mathrm{c}) = 0$ and $\lim_{n\to\infty}(\bar{f} \circ f)^n(z_\mathrm{c}) = z_0$.*

To prove this, we first observe that $h(z_0) = (\bar{f} \circ f)(z_0) = \bar{f}[f(z_0)] = \bar{f}(\bar{z}_0) = \overline{f(z_0)} = z_0$, that is, z_0 is a fixed point of $h(z)$. Next, from the chain rule for the derivative of a composite function,

$$h'(z) = (\bar{f} \circ f)'(z) = \bar{f}'[f(z)]f'(z) = \bar{s}'[f(z)]s'(z), \tag{B1}$$

we find that $h'(z_0) = \bar{s}'[f(z_0)]s'(z_0) = \bar{s}'(\bar{z}_0)s'(z_0) = \overline{s'(z_0)}s'(z_0) = |s'(z_0)|^2$ and so that $|h'(z_0)| < 1$. (Here, $\bar{s}(z) = \overline{s(\bar{z})}$ or equivalently $\bar{s}(z) = \bar{f}(z) - \zeta$.) Then, from Theorem B.2, for each z_0, there exists at least one point z_c such that $h'(z_\mathrm{c}) = 0$ and $\lim_{n\to\infty} h^n(z_\mathrm{c}) = \lim_{n\to\infty}(\bar{f} \circ f)^n(z_\mathrm{c}) = z_0$. From equation (B1), the $h'(z_\mathrm{c}) = 0$ indicates that we have either $\bar{s}'(w_\mathrm{c}) = 0$ where $w_\mathrm{c} = f(z_\mathrm{c})$, or $s'(z_\mathrm{c}) = 0$. If the latter is the case, z_c is simply the point that we are looking for. If the former, we find that $s'(\bar{w}_\mathrm{c}) = \overline{\bar{s}'(w_\mathrm{c})} = 0$ and that

$$\begin{aligned}\lim_{n\to\infty}(\bar{f} \circ f)^n(\bar{w}_\mathrm{c}) &= \lim_{n\to\infty}(\bar{f} \circ f)^n[\overline{f(z_\mathrm{c})}] = \lim_{n\to\infty}(\bar{f} \circ f)^n[\bar{f}(\bar{z}_\mathrm{c})] \\ &= \lim_{n\to\infty} \bar{f}[(f \circ \bar{f})^n(\bar{z}_\mathrm{c})] = \bar{f}\left[\lim_{n\to\infty}(f \circ \bar{f})^n(\bar{z}_\mathrm{c})\right] \\ &= \bar{f}\left[\overline{\lim_{n\to\infty}(\bar{f} \circ f)^n(z_\mathrm{c})}\right] = \bar{f}(\bar{z}_0) = \overline{f(z_0)} = z_0.\end{aligned}$$

Here, we have exploited the associativity of the composition of functions and the commutativity between the limit and the any analytic map. We conclude that $\bar{w}_\mathrm{c}$ is the point that we are looking for. While it is not of direct interest here, following similar arguments, we can further show that, for any point z_0 satisfying the condition part of Theorem B.3, there are at least $(r+1)$ points z_c – where r is the degree of $s(z)$ – such that $h'(z_\mathrm{c}) = 0$ and $\lim_{n\to\infty} h^n(z_\mathrm{c}) = z_0$ (i.e., the consequence part of Theorem B.2). In particular, at least one of them satisfies $s'(z_\mathrm{c}) = 0$, while r of them map to a single point w_c under f – i.e., they are all of the r pre-images of w_c – where w_c satisfies $\bar{s}'(w_\mathrm{c}) = 0$.

Note that the condition part of Theorem B.3 is actually equivalent to z_0 being an actual image position with $\mathscr{J}(z_0) > 0$. That is, $f(z_0) = \zeta + s(z_0) = \bar{z}_0$ so that $\zeta = z_0 - \bar{s}(\bar{z}_0)$, which is just the lens equation, whereas $\mathscr{J}(z_0) = 1 - |s'(z_0)|^2 = (1-|s'(z_0)|)(1+|s'(z_0)|) > 0$ if (and only if) $|s'(z_0)| < 1$. Hence, the immediate corollary of Theorem B.3 is that

Corollary B.4. (Rhie 2001) *The number of positive parity images (n_+) for the lens mapping $\zeta = z - \overline{s(z)}$ that can be described by a rational function $s(z)$ of degree $r \geqslant 2$ is bounded by the number of stationary points of $s(z)$.*

However, it is known that the latter number is exactly $2r-2$, if the point at infinity is included and the multiplicity has been counted,[8] and therefore, $n_+ \leqslant 2(r-1)$ (Rhie 2001; Khavinson & Neumann 2006).

While this limit is strictly correct, the number of *distinct* stationary points of $s(z)$ may be smaller than $2r-2$, if there are degenerate solutions for $s'(z) = 0$. In particular, if there exists a point z_c such that $s'(z_\mathrm{c}) = \ldots = s^{(n-1)}(z_\mathrm{c}) = 0$ and $s^{(n)}(z_\mathrm{c}) \neq 0$ or if $s(z)$ possesses an n-th order pole, with $n \geqslant 3$, the number of distinct stationary points and consequently the limit on n_+ is lowered by $n-2$ for each such point. Another possibility for lowering this limit further depends on the asymptotic behaviour of $s(z)$, provided that we are only interested in images with $|z_0| < \infty$.

- First, if $\lim_{z\to\infty} s(z) = a$ is finite, $z = \infty$ is not a fixed point of $h(z)$ provided that $s(z)$ does not have a pole at $\zeta + \bar{a}$. On the other hand, if $s(z) \sim a + bz^{-n}$ where $b \neq 0$ is a constant and $n \geqslant 3$ is an integer, then $s'(\infty) = \ldots = s^{(n-1)}(\infty) = 0$ and $s^{(n)}(\infty) \neq 0$ so that $z = \infty$ is an $(n-1)$-times degenerate stationary point. Consequently, we lose $(n-2)$ distinct points that might have iteratively converged to one of the positive parity images, and thus, the upper limit on n_+ is lowered to $n_+ \leqslant 2r - n$.
- Secondly, if $s(z)$ diverges at least quadratically, we find not only that $s'(\infty) = h'(\infty) = 0$, but also that $h(\infty) = \infty$. In other words, $z = \infty$ is a stationary point *and* a (super-attracting) fixed point. For this case, the point $z = \infty$ obviously does not iteratively converge to any finite fixed point, and therefore, this point should not be considered for the limit for n_+ at all (counting all of its multiplicity). If $s(z) \sim az^n$ ($a \neq 0$ and $n \geqslant 2$), we find that $s'(\infty) = \ldots = s^{(n-1)}(\infty) = 0$ and $s^{(n)} \neq 0$, and thus, the limit is lowered to $n_+ \leqslant 2r - n - 1$.
- Finally, if $s(z)$ diverges linearly so that $s(z) \sim az$ ($a \neq 0$), then $s'(\infty) = a^{-1} \neq 0$ and $s(\infty) = f(\infty) = \infty$ and consequently, $h'(\infty) = |a|^{-2}$ and $h(\infty) = \infty$. With the identification of $\bar{\infty} = \infty$, we can conclude that there is at least one finite point such that $s'(z_\mathrm{c}) = 0$ and $\lim_{n\to\infty} h^n(z_\mathrm{c}) = \infty$ if $|a| > 1$ since $z = \infty$ is a non-stationary attracting fixed point. Therefore, for $|a| > 1$, there is one less point with $s'(z) = 0$ that can iteratively converge to one of the finite positive parity images, and consequently, the limit is given by $n_+ \leqslant 2r - 3$. However, if $|a| < 1$, the fixed point at infinity is repelling and thus does not affect the behaviour of the iteration of finite points, and the original limit $n_+ \leqslant 2(r-1)$ is maintained.

B1 Index Theorem for a rational lens mapping

The limit on n_+ can be extended to the limit on the number of total images $(n_+ + n_-)$ by deriving the relation between the numbers of positive and negative parity images (n_+ and n_-, respectively). Let us first think of a function $F(z,\bar{z}) = s(z) - \bar{z} - \bar{\zeta}$ and

$$\mathrm{d}\ln F = \frac{\partial_z F \mathrm{d}z + \partial_{\bar{z}} F \mathrm{d}\bar{z}}{F} = \frac{s'(z)\mathrm{d}z - \mathrm{d}\bar{z}}{s(z) - \bar{z} - \bar{\zeta}}.$$

Then, the contour integral

$$\mathrm{i}\,\Delta_{\partial C} \arg F = \oint_{\partial C} \frac{s'(z)\mathrm{d}z - \mathrm{d}\bar{z}}{s(z) - \bar{z} - \bar{\zeta}}$$

along the boundary of a domain $C \subset \mathbb{C}$ vanishes, provided that the domain C does not contain any image position (i.e., zeros of F) nor poles of $s(z)$ [i.e., $s(z) \neq \bar{z} + \bar{\zeta}$ and $|s'(z)| < \infty$ for $\forall z \in C$]. This follows because the integrand is exact, so that it is closed in C. Furthermore, for an arbitrary domain C that may contain image positions and/or poles, the integral can be evaluated by collapsing the contour to infinitesimally small circles around each image position and pole.

Suppose that z_0 is an image position that is not on the critical curve. Then, $s(z) \simeq \bar{\zeta} + \bar{z}_0 + (z - z_0)s'(z_0) + \mathscr{O}(|z - z_0|^2)$ and $s'(z) \simeq$

[8] This follows from the Riemann–Hurwitz formula. That is, since $s(z) : \mathbb{C}_\infty \to \mathbb{C}_\infty$ is an analytic map of degree r of the Riemann sphere (whose Euler characteristic is 2) onto itself, the total number of ramification points (or stationary points) is $2r-2$. In particular, for a polynomial $p(z)$ of order r, its derivative is a polynomial of order $(r-1)$ so there are $(r-1)$ stationary points in $\mathbb{C}$. In addition, since $p(z) \sim az^r$ ($a \neq 0$), the point at infinity is degenerate $(r-1)$ times, and thus it contribute an additional $(r-1)$ counts of ramification points.

Table B1. The number of non-infinite regular images for a rational lens mapping of degree $r \geqslant 2$. Here, the lens equation is given by $\zeta = z - \bar{s}(z)$ with $s(z)$ being a rational function of z of degree $r \geqslant 2$. The asymptotic behaviour of $s(z)$ as $z \to \infty$ determines the maximum possible number of non-infinite positive parity images. The positive integer n is basically the ramification index at infinity. If $s(z)$ is finite at infinity, the total count of the order of poles in $\mathbb{C}$ is the same as the degree r while it is $r - n$ if $s(z)$ diverges at infinity. Physically, the number of poles corresponds to the number of point masses. The positive integer d is the duplication index, which counts the number of $m(\geqslant 3)$-th order poles as well as points such that $s'(z_c) = \ldots = s^{(m-1)}(z_c) = 0$ and $s^{(m)}(z_c) \neq 0$ with $m \geqslant 3$. For each such point contributes $m - 2$ to d.

Asymptotic Behaviour	n_+	$n_- - n_+$	$n_+ + n_-$
$\sim a + bz^{-n}$ ($b \neq 0$ and $n \geqslant 3$)	$\leqslant 2r - n - d$	$r - 1$	$\leqslant 5r - 2n - 1 - 2d$
$\sim a + bz^{-n}$ ($b \neq 0$ and $n = 1, 2$)	$\leqslant 2r - 2 - d$	$r - 1$	$\leqslant 5r - 5 - 2d$
$\sim az$ ($0 < \lvert a\rvert < 1$)	$\leqslant 2r - 2 - d$	$r - 2$	$\leqslant 5r - 6 - 2d$
$\sim az$ ($\lvert a\rvert > 1$)	$\leqslant 2r - 3 - d$	r	$\leqslant 5r - 6 - 2d$
$\sim az^n$ ($a \neq 0$ and $n \geqslant 2$)	$\leqslant 2r - n - 1 - d$	r	$\leqslant 5r - 2n - 2 - 2d$

$s'(z_0) + \mathcal{O}(|z - z_0|)$, and thus, the integral along the small circle $z = z_0 + \epsilon e^{i\varphi}$ ($0 \leqslant \varphi < 2\pi$) around z_0 reduces to

$$i\,\Delta_{\partial C} \arg F = i \int_0^{2\pi} d\varphi\, \frac{s'(z_0)e^{i\varphi} + e^{-i\varphi} + \mathcal{O}(\epsilon)}{s'(z_0)e^{i\varphi} - e^{-i\varphi} + \mathcal{O}(\epsilon)},$$

and can be evaluated as the limiting value for $\epsilon \to 0$. That is, if $|s'(z_0)| < 1$,

$$\int_0^{2\pi} d\varphi\, \frac{s'(z_0)e^{i\varphi} + e^{-i\varphi}}{s'(z_0)e^{i\varphi} - e^{-i\varphi}} = -\int_0^{2\pi} d\varphi\, \frac{1 + s'(z_0)e^{2i\varphi}}{1 - s'(z_0)e^{2i\varphi}} = -2\pi,$$

whereas if $|s'(z_0)| > 1$,

$$\int_0^{2\pi} d\varphi\, \frac{s'(z_0)e^{i\varphi} + e^{-i\varphi}}{s'(z_0)e^{i\varphi} - e^{-i\varphi}} = \int_0^{2\pi} d\varphi\, \frac{1 + [s'(z_0)]^{-1}e^{-2i\varphi}}{1 - [s'(z_0)]^{-1}e^{-2i\varphi}} = 2\pi.$$

Here, both results can be obtained by series-expanding the denominator and using $\int_0^{2\pi} e^{in\varphi} d\varphi = 0$ where n is a non-zero integer.

Similarly, for a pole z_p of $s(z)$ of order n, by factoring out the diverging part, it is possible to write $s(z) = (z - z_p)^{-n} s_p(z)$ where $s_p(z_p)$ is non-zero finite and $s'(z) = -n(z - z_p)^{-n-1} s_p(z) + (z - z_p)^{-n} s_p'(z)$. Consequently, the integral along the small circle around the pole $z = z_p + \epsilon e^{i\varphi}$ ($0 \leqslant \varphi < 2\phi$) is given as

$$i\,\Delta_{\partial C} \arg F = i \int_0^{2\pi} d\varphi\, \frac{-n s_p(z) + \epsilon e^{i\varphi} s_p'(z) + \epsilon^{n+1} e^{(n-1)i\varphi}}{s_p(z) - \epsilon^n e^{ni\varphi}(\bar{\zeta} + \bar{z}_p) - \epsilon^{n+1} e^{(n-1)i\varphi}}$$

the limiting value of which as $\epsilon \to 0$ is $-2n\pi i$, assuming $\lim_{z \to z_p} s_p'(z)$ is finite. Hence, for any domain C chosen large enough to contain all of image positions and poles of $s(z)$ in $\mathbb{C}$, we find that

$$\Delta_{\partial C} \arg F = 2\pi(n_- - n_+ - n_\infty) \tag{B2}$$

where n_+ and n_- are the total numbers of positive [$|s'(z_0)| < 1$ so that $\mathscr{J}(z_0) > 1$] and negative [$|s'(z_0)| > 1$ so that $\mathscr{J}(z_0) < 1$] parity images, respectively, and n_∞ is the sum of orders of all poles. This result is in fact a particular case of the argument principle applied on the function F.

However, for a large enough contour ∂C, the integral can also be evaluated using a contour around the point at infinity

$$i\,\Delta_{\partial C} \arg F = \oint_{\partial C} \frac{s'(z)dz - d\bar{z}}{s(z) - \bar{z} - \bar{\zeta}} = -\oint_{\partial C} \frac{w^{-2}s'(w^{-1})dw - \bar{w}^{-2}d\bar{w}}{s(w^{-1}) - \bar{w}^{-1} - \bar{\zeta}}.$$

The limiting result as $w \to 0$ is dependent on the asymptotic behaviour of $s(z)$ as $z \to \infty$. If $\lim_{z\to\infty} s(z)$ is finite, using the asymptotic expansion form $s(z) \sim a + bz^{-n}$ where a and $b \neq 0$ are constants (a may be nil) and n is a positive integer, the integral reduces to

$$i\,\Delta_{\partial C} \arg F = \oint_{\partial C} \frac{d\bar{w}}{\bar{w}} = -i \int_0^{2\pi} d\varphi = -2\pi i.$$

On the other hand, if $s(z)$ diverges at least quadratically, that is $s(z) \sim az^n$ with $n \geqslant 2$ and $a \neq 0$, then

$$i\,\Delta_{\partial C} \arg F = n \oint_{\partial C} \frac{dw}{w} = ni \int_0^{2\pi} d\varphi = 2n\pi i.$$

Finally, if $s(z) \sim az$ ($a \neq 0$) diverges linearly, then

$$i\,\Delta_{\partial C} \arg F = i \int_0^{2\pi} d\varphi \frac{ae^{-i\varphi} + e^{i\varphi}}{ae^{-i\varphi} - e^{i\varphi}} = \begin{cases} 2\pi i & \text{if } |a| > 1 \\ -2\pi i & \text{if } |a| < 1 \end{cases}.$$

By summarizing the results, we arrive at a relation for the difference between the numbers of positive and negative parity images

$$n_- - n_+ = \begin{cases} n_\infty - 1 & \text{if } \lim_{z\to\infty} |z^{-1}s(z)| < 1 \\ n_\infty + n = r & \text{if } \lim_{z\to\infty} |z^{-1}s(z)| > 1 \end{cases} \tag{B3}$$

where n is the ramification index of $s(z)$ at $z = \infty$. Since $s(z)$ is a rational function, if $s(z)$ diverges as $z \to \infty$, n is the same as the asymptotic power index of $s(z)$, which must be an integer for this case. Furthermore, n_∞ is in fact the same as the order of the polynomial in the denominator when $s(z)$ is expressed as a quotient of relative prime polynomials. Since the asymptotic power index for a rational function is basically the difference of the orders of those polynomials, and the degree of the rational function is the larger of two, we find that $r = n_\infty + n$ if $s(z)$ is divergent as $z \to \infty$. This result is in fact the extension of the so-called index theorem (Burke 1981) to the case when the deflection function is given by a rational function.

The fact that $n_- - n_+$ is a fixed number for given $s(z)$, in particular, being independent of ζ, further implies that for a given lens system, change of source position can only create or destroy images of opposite parity in a pair. The upper limit on the total number of non-infinite images can be directly found from the limit on n_+ using $n_+ + n_- = 2n_+ + (n_- - n_+)$. The final result on the limits of number of images for a number of rational lens maps are summarized in Table B1.

Comparing the upper limit on the number of images to the degree of the imaging equation $g(z) = z - h(z) = 0$, which is either r^2 if $s(z)$ diverges as $z \to \infty$ or $r^2 + 1$ if otherwise, we find that they can be same only if $r = 2$ or $r = 3$ [i.e., $r^2 - 5r + 6 = (r - 2)(r - 3) = 0$]. If $s(z)$ is a non-degenerate Möbius transformation, that is, a degree-1 rational function, explicit calculations can establish that the imaging equation reduces to either a linear equation if $s(z)$ is a linear polynomial, or a quadratic equation if otherwise, with all of its solutions yielding image locations. In other words, the imaging equation must have solutions that are not image locations if $r \geqslant 4$. This also indicates that the moment sum invariants that may be derived through the similar methods as in section 3.1 will be valid only if the degree of the rational deflection function is 1, 2, or 3, since, if otherwise, there must be spurious roots.

APPENDIX C: THE MEAN MAGNIFICATION FOR THE SOURCE INSIDE THE CAUSTICS

As noted in section 5.2, the ratio of the areas under the caustics and the pre-caustics gives the mean magnification for the source inside the caustics. So far, we have derived the areas under the caustics (eqs. 55 and A2) for $0 \leqslant |\gamma| < 1$ and (eqs. 60, A4 and A13) for $|\gamma| > 1$, and under the pre-caustic (eqs. 86, A11 and A16) for $|\gamma| > 1$. To complete the discussion for all values of $|\gamma|$, we need to figure out the area between the two pre-caustics for $0 \leqslant \gamma < 1$ (eqs. 63 and 64). As it turns out, this can be expressed in terms of the standard elliptic integrals (all four forms are equivalent):

$$\begin{aligned}
S[z_{\rm p}^+] - S[z_{\rm p}^-] &= \frac{4|\gamma|}{c^{5/2}}\left[(1+c)\mathbf{\Pi}(\mu,x) + \mathbf{K}(x) - 2c\mathbf{E}(x)\right] \\
&= \frac{4|\gamma|}{c^{5/2}}\left[\frac{|\gamma|^2(1+2c)}{1+c}\mathbf{\Pi}(-\lambda,x) + c(1+2c)\mathbf{K}(x) - 2c\mathbf{E}(x)\right] \\
&= \frac{4|\gamma|}{c^2(1+2c)^{1/2}}\left[4|\gamma|^2\mathbf{\Pi}(\nu,y) + 2c(1+2c)\mathbf{K}(y) - (1+2c)\mathbf{E}(y)\right] \\
&= \frac{4|\gamma|}{c^2(1+2c)^{1/2}}\left[4c\mathbf{\Pi}(-\tau,y) + 2\mathbf{K}(y) - (1+2c)\mathbf{E}(y)\right],
\end{aligned}$$

or in terms of the Carlson symmetric form:

$$\begin{aligned}
S[z_{\rm p}^+] - S[z_{\rm p}^-] &= \frac{4|\gamma|}{c^{5/2}}\left\{(2-c)R_F\left(0,\frac{\delta}{\rho},1\right) - \frac{1}{6}\left[\frac{|\gamma|^2}{c}R_J\left(0,\frac{\delta}{\rho},1,\frac{1}{\rho}\right) + \frac{4|\gamma|^2-3}{(1+2c)}R_D\left(0,\frac{\delta}{\rho},1\right)\right]\right\} \\
&= \frac{4|\gamma|}{c^{5/2}}\left\{R_F\left(0,\frac{\delta}{\rho},1\right) + \frac{1}{6}\left[\frac{(1+2c)|\gamma|^2}{(1+c)^2}R_J\left(0,\frac{\delta}{\rho},1,\delta\right) + \frac{3-4|\gamma|^2}{(1+2c)}R_D\left(0,\frac{\delta}{\rho},1\right)\right]\right\} \\
&= \frac{4|\gamma|}{c^2(1+2c)^{1/2}}\left\{3R_F\left(0,\frac{\rho}{\delta},1\right) - \frac{1}{3}\left[\frac{4|\gamma|^2}{(1+2c)}R_J\left(0,\frac{\rho}{\delta},1,\frac{1}{\delta}\right) + \frac{3-4|\gamma|^2}{(1+2c)}R_D\left(0,\frac{\rho}{\delta},1\right)\right]\right\} \\
&= \frac{4|\gamma|}{c^2(1+2c)^{1/2}}\left[(1+2c)R_F\left(0,\frac{\rho}{\delta},1\right) + \frac{1}{3}\left[\frac{4c|\gamma|^2}{(1+c)^2}R_J\left(0,\frac{\rho}{\delta},1,\rho\right) + \frac{4|\gamma|^2-3}{(1+2c)}R_D\left(0,\frac{\rho}{\delta},1\right)\right]\right\}.
\end{aligned}$$

Here $c = \sqrt{1-|\gamma|^2}$,

$$\lambda = \frac{1}{2(1+c)}, \qquad \mu = \frac{|\gamma|^2}{2c(1+c)}, \qquad x^2 = \frac{3-4|\gamma|^2}{4c(1+2c)}; \qquad \tau = \frac{|\gamma|^2}{(1+c)^2}, \qquad \nu = \frac{1}{1+2c}, \qquad y^2 = \frac{4|\gamma|^2-3}{(1+2c)^2},$$

$$\rho = \frac{\tau}{\mu} = 1-\tau = \frac{1}{1+\mu} = \frac{2c}{1+c}; \qquad \delta = \frac{\lambda}{\nu} = 1-\lambda = \frac{1}{1+\nu} = \frac{1+2c}{2(1+c)}; \qquad 1-x^2 = \frac{\delta}{\rho} = \frac{1+2c}{4c}; \qquad 1-y^2 = \frac{\rho}{\delta} = \frac{4c}{1+2c},$$

and $\mathbf{\Pi}(n,k)$ is the complete elliptic integral of the third kind:

$$\mathbf{\Pi}(n,k) \equiv \int_0^{\pi/2} \frac{{\rm d}\phi}{\left(1+n\sin^2\phi\right)\sqrt{1-k^2\sin^2\phi}}$$

and $R_J(x,y,z,p)$ is an additional Carlson's integral:

$$R_J(x,y,z,p) \equiv \frac{3}{2}\int_0^\infty (t+x)^{-1/2}(t+y)^{-1/2}(t+z)^{-1/2}(t+p)^{-1}dt.$$

Note that $\mathbf{\Pi}(n,k) = R_F(0,1-k^2,1) - (n/3)R_J(0,1-k^2,1,1+n)$. With these results, we can find the analytic expressions for the mean magnification for the source inside the caustics.

As a simple illustration of the use of these expressions, we derive the asymptotic expansions of $\langle M\rangle/M_{\rm min}^{\rm c}$, which are also plotted in the lower panel of Fig. 4:

$$\begin{aligned}
\frac{\langle M\rangle}{M_{\rm min}^{\rm c}} &\simeq \frac{8}{3\pi}\left[3\mathbf{K}\left(\frac{1}{2}\right) - 2\mathbf{E}\left(\frac{1}{2}\right)\right] - \frac{|\gamma|^2}{2\pi}\left[13\mathbf{K}\left(\frac{1}{2}\right) - 14\mathbf{E}\left(\frac{1}{2}\right)\right] - \frac{|\gamma|^4}{288\pi}\left[123\mathbf{K}\left(\frac{1}{2}\right) - 98\mathbf{E}\left(\frac{1}{2}\right)\right] + \mathscr{O}(|\gamma|^6), \qquad (|\gamma| \to 0) \\
\frac{\langle M\rangle}{M_{\rm min}^{\rm c}} &\simeq 1 - \frac{2}{4-\pi+2\ln(c/4)} + \frac{c^2}{2}\left\{\frac{3\pi-8}{4-\pi+2\ln(c/4)} + \frac{10-3\pi}{[4-\pi+2\ln(c/4)]^2}\right\} \\
&\quad + \frac{c^4}{8}\left\{\frac{3}{2} + \frac{15\pi-41}{2[4-\pi+2\ln(c/4)]} - \frac{267\pi-469-36\pi^2}{4[4-\pi+2\ln(c/4)]^2} - \frac{(10-3\pi)^2}{[4-\pi+2\ln(c/4)]^3}\right\} + \mathscr{O}(c^6), \qquad (|\gamma| \to 1^-) \\
\frac{\langle M\rangle}{M_{\rm min}^{\rm c}} &\simeq 1 - \frac{1}{2+\ln(q/4)} - \frac{q^2}{4}\left\{10 - \frac{14}{2+\ln(q/4)} + \frac{3}{[2+\ln(q/4)]^2}\right\} \\
&\quad + \frac{q^4}{128}\left\{392 - \frac{724}{2+\ln(q/4)} + \frac{357}{[2+\ln(q/4)]^2} - \frac{72}{[2+\ln(q/4)]^3}\right\} + \mathscr{O}(q^6), \qquad (|\gamma| \to 1^+) \\
\frac{\langle M\rangle}{M_{\rm min}^{\rm c}} &\simeq 2 + \frac{1}{4|\gamma|^2} - \frac{1}{64|\gamma|^4} + \mathscr{O}(|\gamma|^{-6}) \qquad (|\gamma| \to \infty).
\end{aligned}$$

Here, $c^2 = 1 - |\gamma|^2$ and $q^2 = 1 - |\gamma|^{-2}$. For the first two cases ($0 \leqslant |\gamma| < 1$), we have $M^{\rm c}_{\rm min} = [|\gamma|(1 - |\gamma|^2)]^{-1}$ while for the last two cases ($|\gamma| > 1$), $M^{\rm c}_{\rm min} = (2|\gamma|^2 - 1)/(|\gamma|^2 - 1)$.

This paper has been typeset from a TEX/ LATEX file prepared by the author.